33. van Es, M.A., van Vught, P.W., Blauw, H.M., Franke, L., Saris, C.G., Van den Bosch, L., de Jong, S.W., de Jong, V., Baas, F., van't Slot, R. *et al.* (2008) Genetic variation in DPP6 is associated with susceptibility to amyotrophic lateral sclerosis. *Nat. Genet.*, **40**, 29–31.
34. van Es, M.A., Veldink, J.H., Saris, C.G., Blauw, H.M., van Vught, P.W., Birve, A., Lemmens, R., Schelhaas, H.J., Groen, E.J., Huisman, M.H. *et al.* (2009) Genome-wide association study identifies 19p13.3 (UNC13A) and 9p21.2 as susceptibility loci for sporadic amyotrophic lateral sclerosis. *Nat. Genet.*, **41**, 1083–1087.
35. Landers, J.E., Melki, J., Meininger, V., Glass, J.D., van den Berg, L.H., van Es, M.A., Sapp, P.C., van Vught, P.W., McKenna-Yasek, D.M., Blauw, H.M. *et al.* (2009) Reduced expression of the Kinesin-Associated Protein 3 (KIFAP3) gene increases survival in sporadic amyotrophic lateral sclerosis. *Proc. Natl Acad. Sci. USA*, **106**, 9004–9009.
36. Fernandez-Santiago, R., Sharma, M., Berg, D., Illig, T., Anneser, J., Meyer, T., Ludolph, A. and Gasser, T. (2009) No evidence of association of FLJ10986 and ITPR2 with ALS in a large German cohort. *Neurobiol. Aging*, **32**, 551e1–551e4.
37. Fogh, I., D'Alfonso, S., Gellera, C., Ratti, A., Cereda, C., Penco, S., Corrado, L., Soraru, G., Castellotti, B., Tiloca, C. *et al.* (2009) No association of DPP6 with amyotrophic lateral sclerosis in an Italian population. *Neurobiol. Aging*, **32**, 966–967.
38. Chiò, A., Schymick, J.C., Restagno, G., Scholz, S.W., Lombardo, F., Lai, S.L., Mora, G., Fung, H.C., Britton, A., Arepalli, S. *et al.* (2009) A two-stage genome-wide association study of sporadic amyotrophic lateral sclerosis. *Hum. Mol. Genet.*, **18**, 1524–1532.
39. Daoud, H., Belzil, V., Desjarlais, A., Camu, W., Dion, P.A. and Rouleau, G.A. (2010) Analysis of the UNC13A gene as a risk factor for sporadic amyotrophic lateral sclerosis. *Arch. Neurol.*, **67**, 516–517.
40. Laaksovirta, H., Peuralinna, T., Schymick, J.C., Scholz, S.W., Lai, S.L., Myllykangas, L., Sulkava, R., Jansson, L., Hernandez, D.G., Gibbs, J.R. *et al.* (2010) Chromosome 9p21 in amyotrophic lateral sclerosis in Finland: a genome-wide association study. *Lancet Neurol.*, **9**, 978–985.
41. Shatunov, A., Mok, K., Newhouse, S., Weale, M.E., Smith, B., Vance, C., Johnson, L., Veldink, J.H., van Es, M.A., van den Berg, L.H. *et al.* (2010) Chromosome 9p21 in sporadic amyotrophic lateral sclerosis in the UK and seven other countries: a genome-wide association study. *Lancet Neurol.*, **9**, 986–994.
42. Iida, A., Takahashi, A., Deng, M., Zhang, Y., Wang, J., Atsuta, N., Tanaka, F., Kamei, T., Sano, M., Oshima, S. *et al.* (2011) Replication analysis of SNPs on 9p21.2 and 19p13.3 with amyotrophic lateral sclerosis in East Asians. *Neurobiol. Aging*, **32**, 757e13–757e14.
43. Haga, H., Yamada, R., Ohnishi, Y., Nakamura, Y. and Tanaka, T. (2002) Gene-based SNP discovery as part of the Japanese Millennium Genome Project: identification of 190,562 genetic variations in the human genome. Single-nucleotide polymorphism. *J. Hum. Genet.*, **47**, 605–610.
44. Henrich-Noack, P., Prehn, J.H. and Krieglstein, J. (1994) Neuroprotective effects of TGF-beta 1. *J. Neural. Transm. Suppl.*, **43**, 33–45.
45. Iwasaki, Y., Shiojima, T., Tagaya, N., Kobayashi, T. and Kinoshita, M. (1997) Effect of transforming growth factor beta 1 on spinal motor neurons after axotomy. *J. Neurol. Sci.*, **147**, 9–12.
46. Krieglstein, K., Strelau, J., Schober, A., Sullivan, A. and Unsicker, K. (2002) TGF-beta and the regulation of neuron survival and death. *J. Physiol. Paris*, **96**, 25–30.
47. Ozaki, K., Ohnishi, Y., Iida, A., Sekine, A., Yamada, R., Tsunoda, T., Sato, H., Hori, M., Nakamura, Y. and Tanaka, T. (2002) Functional SNPs in the lymphotoxin-alpha gene that are associated with susceptibility to myocardial infarction. *Nat. Genet.*, **32**, 650–654.
48. Kubo, M., Hata, J., Ninomiya, T., Matsuda, K., Yonemoto, K., Nakano, T., Matsushita, T., Yamazaki, K., Ohnishi, Y., Saito, S. *et al.* (2007) A nonsynonymous SNP in PRKCH (protein kinase C eta) increases the risk of cerebral infarction. *Nat. Genet.*, **39**, 212–217.
49. Tomlinson, I.P., Webb, E., Carvajal-Carmona, L., Broderick, P., Howarth, K., Pittman, A.M., Spain, S., Lubbe, S., Walther, A., Sullivan, K. *et al.* (2008) A genome-wide association study identifies colorectal cancer susceptibility loci on chromosomes 10p14 and 8q23.3. *Nat. Genet.*, **40**, 623–630.
50. Miyamoto, Y., Shi, D., Nakajima, M., Ozaki, K., Sudo, A., Kotani, A., Uchida, A., Tanaka, T., Fukui, N., Tsunoda, T. *et al.* (2008) Common variants in DVWA on chromosome 3p24.3 are associated with susceptibility to knee osteoarthritis. *Nat. Genet.*, **40**, 994–998.
51. Suppiah, V., Moldovan, M., Ahlenstiel, G., Berg, T., Weltman, M., Abate, M.L., Bassendine, M., Spengler, U., Dore, G.J., Powell, E. *et al.* (2009) IL28B is associated with response to chronic hepatitis C interferon-alpha and ribavirin therapy. *Nat. Genet.*, **41**, 1100–1104.
52. Price, A.L., Patterson, N.J., Plenge, R.M., Weinblatt, M.E., Shadick, N.A. and Reich, D. (2006) Principal components analysis corrects for stratification in genome-wide association studies. *Nat. Genet.*, **38**, 904–909.
53. Weir, B.S. (1996) *Genetic Data Analysis II*. Sinauer Associates, Sunderland.
54. Colland, F., Jacq, X., Trouplin, V., Mougin, C., Groizeleau, C., Hamburger, A., Meil, A., Wojcik, J., Legrain, P. and Gauthier, J.M. (2004) Functional proteomics mapping of a human signaling pathway. *Genome Res.*, **14**, 1324–1332.
55. Zawel, L., Dai, J.L., Buckhaults, P., Zhou, S., Kinzler, K.W., Vogelstein, B. and Kern, S.E. (1998) Human Smad3 and Smad4 are sequence-specific transcription activators. *Mol. Cell*, **1**, 611–617.
56. Nagase, T., Ishikawa, K., Kikuno, R., Hirosawa, M., Nomura, N. and Ohara, O. (1999) Prediction of the coding sequences of unidentified human genes. XV. The complete sequences of 100 new cDNA clones from brain which code for large proteins in vitro. *DNA Res.*, **6**, 337–345.
57. Docagne, F., Nicole, O., Gabriel, C., Fernandez-Monreal, M., Lesne, S., Ali, C., Plawinski, L., Carmeliet, P., MacKenzie, E.T., Buisson, A. *et al.* (2002) Smad3-dependent induction of plasminogen activator inhibitor-1 in astrocytes mediates neuroprotective activity of transforming growth factor-beta 1 against NMDA-induced necrosis. *Mol. Cell Neurosci.*, **21**, 634–644.
58. Houi, K., Kobayashi, T., Kato, S., Mochio, S. and Inoue, K. (2002) Increased plasma TGF-beta1 in patients with amyotrophic lateral sclerosis. *Acta Neurol. Scand.*, **106**, 299–301.
59. Jiang, Y.M., Yamamoto, M., Kobayashi, Y., Yoshihara, T., Liang, Y., Terao, S., Takeuchi, H., Ishigaki, S., Katsuno, M., Adachi, H. *et al.* (2005) Gene expression profile of spinal motor neurons in sporadic amyotrophic lateral sclerosis. *Ann. Neurol.*, **57**, 236–251.
60. Nakamura, M., Ito, H., Wate, R., Nakano, S., Hirano, A. and Kusaka, H. (2008) Phosphorylated Smad2/3 immunoreactivity in sporadic and familial amyotrophic lateral sclerosis and its mouse model. *Acta Neuropathol.*, **115**, 327–334.
61. Ilzecka, J., Stelmasiak, Z. and Dobosz, B. (2002) Transforming growth factor-Beta 1 (tgf-Beta 1) in patients with amyotrophic lateral sclerosis. *Cytokine*, **20**, 239–243.
62. Brooks, B.R., Miller, R.G., Swash, M. and Munsat, T.L. (2000) El Escorial revisited: revised criteria for the diagnosis of amyotrophic lateral sclerosis. *Amyotroph. Lateral Scler. Other Motor Neuron Disord.*, **1**, 293–299.
63. Nakamura, Y. (2007) The BioBank Japan Project. *Clin. Adv. Hematol. Oncol.*, **5**, 696–697.
64. Ohnishi, Y., Tanaka, T., Ozaki, K., Yamada, R., Suzuki, H. and Nakamura, Y. (2001) A high-throughput SNP typing system for genome-wide association studies. *J. Hum. Genet.*, **46**, 471–477.
65. Tsunoda, T., Lathrop, G.M., Sekine, A., Yamada, R., Takahashi, A., Ohnishi, Y., Tanaka, T. and Nakamura, Y. (2004) Variation of gene-based SNPs and linkage disequilibrium patterns in the human genome. *Hum. Mol. Genet.*, **13**, 1623–1632.
66. Saito, A. and Kamatani, N. (2002) Strategies for genome-wide association studies: optimization of study designs by the stepwise focusing method. *J. Hum. Genet.*, **47**, 360–365.
67. International HapMap Consortium. (2005) A haplotype map of the human genome. *Nature*, **437**, 1299–1320.
68. Andrews, N.C. and Faller, D.V. (1991) A rapid micropreparation technique for extraction of DNA-binding proteins from limiting numbers of mammalian cells. *Nucleic Acids Res.*, **19**, 2499.

ELSEVIER

Neurobiology of Aging 32 (2011) 757.e13–757.e14

NEUROBIOLOGY OF AGING

www.elsevier.com/locate/neuaging

Negative results

Replication analysis of SNPs on 9p21.2 and 19p13.3 with amyotrophic lateral sclerosis in East Asians

Aritoshi Iida[a], Atsushi Takahashi[b], Min Deng[c], Yun Zhang[c], Jing Wang[c], Naoki Atsuta[d], Fumiaki Tanaka[d], Tetsumasa Kamei[e], Motoki Sano[f], Shuichi Oshima[g], Torao Tokuda[h], Mitsuya Morita[i], Chizuru Akimoto[i], Masahiro Nakajima[a], Michiaki Kubo[j], Naoyuki Kamatani[b], Imaharu Nakano[i], Gen Sobue[d], Yusuke Nakamura[k,l], Dongsheng Fan[c,**], Shiro Ikegawa[a,*]

[a] *Laboratory for Bone and Joint Diseases, Center for Genomic Medicine, RIKEN, Tokyo, Japan*
[b] *Laboratory for Statistical Analysis, Center for Genomic Medicine, RIKEN, Tokyo, Japan*
[c] *Department of Neurology, Peking University Third Hospital, Beijing, China*
[d] *Department of Neurology, Graduate School of Medicine, Nagoya University, Aichi, Japan*
[e] *Department of Neurology, Chigasaki Tokushukai General Hospital, Kanagawa, Japan*
[f] *Department of Neurology, Chibanishi General Hospital, Chiba, Japan*
[g] *Department of Neurosurgery, Chiba Tokushukai Hospital, Chiba, Japan*
[h] *Tokushukai Group, Tokyo, Japan*
[i] *Division of Neurology, Department of Medicine, Jichi Medical University, Tochigi, Japan*
[j] *Laboratory for Genotyping Development, Center for Genomic Medicine, RIKEN, Kanagawa, Japan*
[k] *Laboratory for International Alliance, Center for Genomic Medicine, RIKEN, Kanagawa, Japan*
[l] *Laboratory of Molecular Medicine, Human Genome Center, Institute of Medical Science, The University of Tokyo, Tokyo, Japan*

Received 29 September 2010; received in revised form 11 December 2010; accepted 21 December 2010

Abstract

We performed a replication study of the 2 genetic variants, rs2814707 on 9p21.2 and rs12608932 on 19p13.3 that are recently reported to be most significantly associated with sporadic amyotrophic lateral sclerosis (ALS) in Caucasians. Both rs12608932 and rs2814707 showed no evidence of association in Japanese and Chinese (rs12608932, combined $p = 0.58$, odds ratio [OR] = 1.03, 95% confidence interval [CI] 0.93–1.13; rs2814707, combined $p = 0.88$, OR = 1.10, 95% CI 0.93–1.30). The association of these loci with susceptibility to sporadic ALS is considered negative in East Asians.

Keywords: Amyotrophic lateral sclerosis; Single nucleotide polymorphism; Genome-association study; Replication study; UNC13A; 9p21.2

Recently, van Es et al. (2009) identified 2 loci significantly associated with sporadic amyotrophic lateral sclerosis (ALS) in Caucasians. The genome-wide level association was identified on 3 single nucleotide polymorphisms (SNPs), in the order of significance, rs12608932 on chromosome 19p13.3 and rs2814707 and rs3849942 on chromosome 9p21.2. In this study, we checked replication of the association of the 2 loci in Japanese (1179 cases and 1645 controls) and Chinese (684 cases and 830 controls) cohorts by examining the most significantly associated SNPs (rs12608932 and rs2814707) in the previous study (van Es et al., 2009). Detailed materials and methods are described in Supplementary data.

* Corresponding author at: Laboratory for Bone and Joint Diseases, Center for Genomic Medicine, RIKEN, Institute of Medical Science, The University of Tokyo, 4-6-1 Shirokanedai, Minato-ku, Tokyo 108-8639, Japan. Tel.: +81 3 5449 5393; fax: +81 3 5449 5393.
E-mail address: sikegawa@ims.u-tokyo.ac.jp (S. Ikegawa).
** Alternate corresponding author at: Department of Neurology, Peking University Third Hospital, 49 North Garden Road, Haidian District, Beijing 100191, China.
E-mail address: dsfan@yahoo.cn (D. Fan).

0197-4580/$ – see front matter © 2011 Elsevier Inc. All rights reserved.
doi:10.1016/j.neurobiolaging.2010.12.011

The allele frequency of rs12608932 was different between Caucasians and East Asians (Supplementary Table 1). The association in Japanese did not reach statistical significance by a logistic regression analysis ($p = 0.67$, odds ratio [OR] = 1.02, 95% confidence interval [CI] 0.91–1.16). Similarly, no association of rs12608932 with sporadic ALS was detected in Chinese ($p = 0.73$, OR = 1.02, 95% CI 0.88–1.20). We then calculated combined p value for the Japanese and Chinese studies by an inverse variance method and observed no association in the East Asians ($p = 0.58$, OR = 1.03, 95% CI 0.93–1.13).

We found that rs2814707 was not associated with susceptibility to sporadic ALS in Japanese and Chinese (Supplementary Table 1). The meta-analysis showed that there was no evidence for the association between rs2814707 and risk of sporadic ALS in East Asians ($p = 0.88$, OR = 1.10, 95% CI 0.93–1.30). However, because the power of the study was less than 80%, this negative association may be due to lack of power that resulted from the limited sample size and/or low risk allele frequency in East Asians. The association between rs2814707 and sporadic ALS in East Asians requires confirmation in further replication studies.

Appendix A. Supplementary data

Supplementary data associated with this article can be found, in the online version, at doi:10.1016/j.neurobiolaging.2010.12.011.

Reference

van Es, M.A., Veldink, J.H., Saris, C.G., Blauw, H.M., van Vught, P.W., Birve, A., Lemmens, R., Schelhaas, H.J., Groen, E.J., Huisman, M.H., van der Kooi, A.J., de Visser, M., Dahlberg, C., Estrada, K., Rivadeneira, F., Hofman, A., Zwarts, M.J., van Doormaal, P.T., Rujescu, D., Strengman, E., Giegling, I., Muglia, P., Tomik, B., Slowik, A., Uitterlinden, A.G., Hendrich, C., Waibel, S., Meyer, T., Ludolph, A.C., Glass, J.D., Purcell, S., Cichon, S., Nöthen, M.M., Wichmann, H.E., Schreiber, S., Vermeulen, S.H., Kiemeney, L.A., Wokke, J.H., Cronin, S., McLaughlin, R.L., Hardiman, O., Fumoto, K., Pasterkamp, R.J., Meininger, V., Melki, J., Leigh, P.N., Shaw, C.E., Landers, J.E., Al-Chalabi, A., Brown, R.H., Jr, Robberecht, W., Andersen, P.M., Ophoff, R.A., van den Berg, L.H., 2009. Genome-wide association study identifies 19p13.3 (UNC13A) and 9p21.2 as susceptibility loci for sporadic amyotrophic lateral sclerosis. Nat. Genet. 41, 1083–1087.

Neurobiology of Disease 45 (2012) 862–870

Contents lists available at SciVerse ScienceDirect

Neurobiology of Disease

journal homepage: www.elsevier.com/locate/ynbdi

Oxidative stress induced by glutathione depletion reproduces pathological modifications of TDP-43 linked to TDP-43 proteinopathies

Yohei Iguchi [a], Masahisa Katsuno [a], Shinnosuke Takagi [a], Shinsuke Ishigaki [a,d], Jun-ichi Niwa [b], Masato Hasegawa [c], Fumiaki Tanaka [a], Gen Sobue [a,d,*]

[a] Department of Neurology, Nagoya University Graduate School of Medicine, 65 Tsurumai-cho, Showa-ku, Nagoya 466–8550, Japan
[b] Stroke Center, Aichi Medical University, Aichi 480–1195, Japan
[c] Departments of Molecular Neurobiology, Tokyo Institute of Psychiatry, Tokyo Metropolitan Organization for Medical Research, 2-1-8 Kamikitazawa, Setagaya-ku, Tokyo 156–8585, Japan
[d] CREST, Japan Science and Technology Agency, 4-1-8, Honcho, Kawaguchi, Saitama 332–0012, Japan

ARTICLE INFO

Article history:
Received 30 March 2011
Revised 29 August 2011
Accepted 4 December 2011
Available online 13 December 2011

Keywords:
TAR DNA-binding protein 43 kDa (TDP-43)
TDP-43 proteinopathy
Oxidative stress
Glutathione depletion
Post-translational modification
Protein phosphorylation

ABSTRACT

TAR DNA-binding protein 43 (TDP-43) is a major component of ubiquitin-positive inclusion of TDP-43 proteinopathies including amyotrophic lateral sclerosis and frontotemporal lobar degeneration with ubiquitinated inclusions, which is now referred to as FTLD-TDP. TDP-43 in the aberrant inclusion is known to be hyperphosphorylated at C-terminal sites, to be truncated at the N-terminal region, and to re-distribute from nucleus to cytoplasm or neurite. The pathogenic role of these modifications, however, has not been clarified. Furthermore, there is no evidence about the initial cause of these modifications. Herein we show that ethacrynic acid (EA), which is able to increase cellular oxidative stress through glutathione depletion, induces TDP-43 C-terminal phosphorylation at serine 403/404 and 409/410, insolubilization, C-terminal fragmentation, and cytoplasmic distribution in NSC34 cells and primary cortical neurons. In the investigation using a nonphosphorylable mutant of TDP-43, there was no evidence that C-terminal phosphorylation of TDP-43 contributes to its solubility or distribution under EA induction. Our findings suggest that oxidative stress induced by glutathione depletion is associated with the process of the pathological TDP-43 modifications and provide new insight for TDP-43 proteinopathies.

Introduction

TAR DNA-binding protein 43 (TDP-43) is a major component of ubiquitin-positive inclusion, a pathological hallmark of TDP-43 proteinopathies including amyotrophic lateral sclerosis (ALS) and frontotemporal lobar degeneration with ubiquitinated inclusions, which is now referred to as FTLD-TDP (Arai et al., 2006; Neumann et al., 2006). Both diseases occur in sporadic or familial forms, and are characterized by late-onset progressive deterioration of motor and/or cognitive function. TDP-43 is a heterogeneous nuclear ribonucleoprotein (hnRNP), which is known to regulate gene transcription and exon splicing through interactions with RNA, hnRNPs, and nuclear bodies (Ayala et al., 2005; Buratti et al., 2005; Wang et al., 2002, 2004). In addition, this protein has also been reported to stabilize human low molecular weight neurofilament (hNFL) mRNA through direct interaction with its 3'UTR (Strong et al., 2007), regulate retinoblastoma protein phosphorylation through the repression of cyclin-dependent kinase 6 (Cdk6) expression (Ayala et al., 2008), regulate activity of Rho family GTPases (Iguchi et al., 2009), and alter the expression of selected microRNAs, such as let-7b and miR-663 (Buratti et al., 2010). Furthermore, very recent works using cross-linking immunoprecipitation sequencing show that multiple RNAs interact with TDP-43 (Polymenidou et al., 2011; Sephton et al., 2011; Tollervey et al., 2011).

Although it mostly localizes in the nucleus under normal conditions, TDP-43 is distributed from nucleus to cytoplasm or neurite, and forms aggregates consisting mainly of C-terminal fragments in affected neurons of patients with TDP-43 proteinopathies. In addition, TDP-43 in the aberrant aggregation is hyperphosphorylated at multiple C-terminal sites (Hasegawa et al., 2008). However, neither the pathogenic role nor the initial cause of these abnormal modifications of TDP-43 has been elucidated. The fact that the majority of patients with TDP-43 proteinopathies are sporadic suggests that exogenous factors induce post-translational modifications of TDP-43 that are seen in the disease. Furthermore, TDP-43 inclusions have also been observed in Alzheimer disease (AD), Parkinson disease (PD),

Abbreviations: TDP-43, TAR DNA-binding protein of 43 kDa; ALS, amyotrophic lateral sclerosis; hnRNP, heterogeneous nuclear ribonucleoprotein; hNFL, human low molecular weight neurofilament; Cdk6, cyclin-dependent kinase 6; ROS, reactive oxygen species; EA, ethacrynic acid; NAC, N-acetylcysteine; CK1, casein kinase 1; CK2, casein kinase 2; WT-TDP-43, wild type TDP-43; SA-TDP-43, nonphosphorylable TDP-43.

* Corresponding author at: Department of Neurology, Nagoya University Graduate School of Medicine, 65 Tsurumai-cho, Showa-ku, Nagoya 466–8550, Japan. Fax: +81 52 744 2785.
E-mail address: sobueg@med.nagoya-u.ac.jp (G. Sobue).
Available online on ScienceDirect (www.sciencedirect.com).

0969-9961/$ – see front matter © 2011 Elsevier Inc. All rights reserved.
doi:10.1016/j.nbd.2011.12.002

dementia with Lewy bodies (DLB), and Huntington disease (HD), argyrophilic grain disease, suggesting that the aggregation of this protein may be a secondary feature of neurodegeneration (Amador-Ortiz et al., 2007; Arai et al., 2009, 2010; Geser et al., 2008; Hasegawa et al., 2007). These findings complicate understanding of the pathogenic role of TDP-43. On the other hand, there is considerable evidence that reactive oxygen species (ROS) and oxidative stress are associated with many neurodegenerative conditions including ALS (Abe et al., 1995, 1997; Beal et al., 1997; Butterfield et al., 2007; Ferrante et al., 1997; Lovell and Markesbery, 2007; Nunomura et al., 2002; Shaw et al., 1995). Herein we show that oxidative stress induced by glutathione depletion reproduces the pathological modifications of TDP-43, that are seen in TDP-43 proteinopathies, in motor neuron-like cells and primary cortical neurons.

Materials and methods

Cell culture and treatment

Mouse NSC34 motor neuron-like cells (a kind gift of N.R. Cashman, University of British Columbia, Vancouver, Canada) were cultured in a humidified atmosphere of 95% air-5% CO2 in a 37 °C incubator in Dulbecco's Modified Eagle's Medium (DMEM) supplemented with 10% fetal bovine serum (FBS). To differentiate the cells, the medium was changed to DMEM containing 1% FBS and 1% NEAA, and was cultured for 24 h. For the interventions, the cells were then incubated with ethacrynic acid (EA) (Sigma-Aldrich, St. Louis, MO), with or without N-acetylcysteine (NAC) (Sigma-Aldrich), casein kinase 1 (CK1) inhibitor (D4476), or casein kinase 2 (CK2) inhibitor (TBCA) (Sigma-Aldrich). Primary cultures of mouse embryonic cortical neurons that were dissociated from embryonic cortex of embryonic day 15 (E15) C57BL/6 J pregnant mice were plated onto poly-L-lysine-coated plates or glass bottom dishes, and maintained in neuron culture medium (Sumilon, Osaka, Japan). Five days after the incubation, the indicated interventions were performed. In both NSC34 cells and primary cortical neurons, the transfections of the intended plasmids were performed using Lipofectamine 2000 (Invitrogen, Eugene, OR), according to the manufacturer's instructions.

DNA constructs

Human wild type TDP-43 (WT-TDP-43) (accession number NM 007375) cDNA was amplified by PCR from cDNA of human spinal cord using the following primers: 5′-CACCATGTCTGAATATATTCGGGTAAC-3′ and 5′-CTACATTCCCCAGCCAGAAGACTTAGAAT-3′. The PCR product was cloned into the pENTR/D-TOPO vector (Invitrogen). For nonphosphorylable TDP-43 (SA-TDP-43) vector, primers containing the mutant substitution of TDP-43 serine 403/404 and 409/410 to alanine were used to mutagenize WT-TDP-43 (KOD-Plus-Mutagenesis kit; Toyobo, Osaka, Japan). The entry vector of WT- or SA-TDP-43 was transferred into pcDNA6.2/N-EmGFP-DEST Vector or pcDNA3.1/nV5-DEST using Gateway LR Clonase II enzyme mix (Invitrogen). The sequences of all constructs were verified using CEQ 8000 genetic analysis system (Beckman Coulter, Brea, CA).

Immunoblot analysis

For whole lysate analysis, NSC34 cells and primary cortical neurons were lysed in 2% SDS sample buffer. For analysis of protein solubility, cells cultured in 6-well plates were lysed in 100 μl of Tris (TS) buffer (50 mM Tris–HCl buffer, pH 7.5, 0.15 M NaCl, 5 mM EDTA, 5 mM EGTA, protein phosphatase inhibitors, and protease inhibitor cocktail). Lysates were sonicated and centrifuged at 100,000 ×g for 15 min. To prevent carryover, the pellets were washed with TS buffer, followed by sonication and centrifugation. TS-insoluble pellets were lysed in 50 μl of Triton-X100 (TX) buffer (TS buffer containing 1% Triton X-100), sonicated, and centrifuged at 100,000 g for 15 min. The pellets were washed with TX buffer, followed by sonication and centrifuge. TX-insoluble pellets were lysed in 50 μl of Sarkosyl (Sar) buffer (TS buffer containing 1% Sarkosyl), sonicated and centrifuged at 100,000 × g for 15 min. Sar-insoluble pellets were lysed in 25 μl of SDS sample buffer. After denaturation, 3 μl of each cell lysate was separated by SDS-PAGE (5%–20% gradient gel) and analyzed by western blotting with ECL Plus detection reagents (GE Healthcare, Buckinghamshire, UK). Primary antibodies used were as follows: anti-TDP-43 rabbit polyclonal antibody (1:1000, ProteinTech, Chicago, IL), anti-TDP-43 (405–414) rabbit polyclonal antibody (1:1000, Cosmo Bio Co. Ltd., Tokyo, Japan), anti-TDP-43 (phospho Ser403/404, Cosmo Bio) rabbit polyclonal antibody (1:1000, Cosmo Bio), anti-TDP-43 (phospho Ser409/410, Cosmo Bio) rabbit polyclonal antibody (1:1000, Cosmo Bio), anti-GAPDH mouse monoclonal antibody (1:2000, Temecula, CA), anti-GFP mouse monoclonal antibody (1:2000, MBL, Nagoya, Japan), and anti-V5 mouse monoclonal antibody (1:2000, Invitrogen).

Assay of ROS production

NSC34 cells to be treated with intended agents were incubated in 96-well plates with 5-(and-6)-chloromethyl-2′,7′-dichlorodihydro fluoresceindiacetate acetyl ester (CM-H2DCFDA) (Molecular Probes, Eugene, OR, USA) for 1 h. Oxidation in the cells was then measured in a multiple-plate reader (PowerscanHT, Dainippon Pharmaceutical, Japan) at excitation and emission wavelengths of 485 nm and 530 nm, respectively. The assays were carried out in 6 wells for each condition.

Immunocytochemistry

NSC34 cells and primary cortical neurons were fixed with 4% paraformaldehyde, incubated with PBS containing 0.2% Triton X-100 for 5 min, blocked, and incubated overnight with anti-TDP-43 rabbit polyclonal antibody (1:1000, ProteinTech), anti-TDP-43 (phospho Ser409/410) mouse monoclonal antibody (1:2000, Cosmo Bio) and anti-TIAR mouse monoclonal antibody (1:1000, BD Transduction Laboratories, Milan, Italy). After washing, samples were incubated with Alexa-488-conjugated goat anti-rabbit IgG (1:1000, Invitrogen) and Alexa-564-conjugated goat anti-mouse IgG (1:1000, Invitrogen) for 30 min, mounted with (Vector Laboratories, Inc. Burlingame, CA), then imaged with a laser conforcal microscope (Nikon A1, Nikon, Tokyo, Japan).

Time lapse analysis

NSC34 cells or mouse primary cortical neurons were grown on glass base dishes, transfected with GFP-WT-TDP-43, and treated with EA. GFP and phase contrast imaging was done every 10 min using a 40X objective lens on a laser scanning confocal microscope.

Cell viability analysis

The 3-(4,5-dimethylthiazol-2-yl)-5-(3-caboxymethoxyphenyl)-2-(4-sulfophenyl)-2H -tetrazolium (MTS)-based cell proliferation assay (MTS assay) was carried out using the CellTiter 96 Aqueous One Solution Cell Proliferation Assay (Promega, Madison, WI), according to the manufacturer's instructions. Absorbance at 490 nm was measured in a multiple-plate reader (PowerscanHT, Dainippon Pharmaceutical, Japan). The assays were carried out in 6 wells for each condition.

Statistical analysis

Statistical differences were analyzed by ANOVA and Bonferroni post hoc analyses for three group comparisons (SPSS version 15.0, SPSS Inc., Chicago, IL). Two-tailed $p<0.05$ was regarded as statistically significant.

Results

EA-mediated oxidative stress induces TDP-43 phosphorylation in NSC34 cells

To investigate the effect of oxidative stress on endogenous TDP-43, NSC34 cells were incubated for 12 h with EA, which is able to increase cellular oxidative stress through depletion of glutathione, (Keelan et al., 2001; Rizzardini et al., 2003). Immunoblots showed abnormal TDP-43-immunoreactive bands at 45 kDa, which suggests hyperphosphorylation of TDP-43, at EA concentration greater than 50 μM EA (Fig. 1A). The bands were immunopositive for phospho-TDP-43-specific (pTDP-43) antibodies at serine 403/404 and serine 409/410 (S403/404 and S409/410), that are seen in TDP-43 proteinopathies as pathological phosphorylation (Hasegawa et al., 2008) (Fig. 1A). In addition, phosphorylation of these TDP-43 sites was prevented by co-treatment with 2 mM NAC, a precursor of glutathione. Quantification of CM-H2DCFDA oxidation, a measure of ROS formation, showed that ROS productions was increased by EA treatment in a dose-dependent manner and was prevented by NAC (Fig. 1B). Since TDP-43 phosphorylation at S403/404 and S409/410 is exerted by CK1 and CK2 (Hasegawa et al., 2008), the effect of treatment with these inhibitors in combination with EA was examined. Both inhibitors prevented serine phosphorylation of TDP-43 in a dose-dependent manner, although CK1 inhibitor was more effective than CK2 inhibitor (Fig. 1C).

EA induces TDP-43 insolubilization and C-terminal fragmentation

To investigate the effect of oxidative stress on endogenous TDP-43 solubility, cells treated with 70 μM EA were extracted sequentially. In the immunoblots, the amount of TDP-43 in TS and TX fractions were significantly decreased, but the amount in Sar and SDS fractions were increased in a time-dependent manner (Fig. 2A). These phenomena were prevented in the presence of 2 mM NAC. Phosphorylated TDP-43 was increased in Sar fractions in a time-dependent manner and was detectable in SDS fractions 5 h after EA induction (Fig. 2A). In addition, long exposure of immunoblots with anti-TDP-43 antibody demonstrated that ~25 kDa C-terminal fragment (CTF) of TDP-43 in Sar and SDS fractions appeared evidently by EA induction, and the amount of TDP-43 CTF in SDS fraction was significantly increased at 5 h after EA induction compared with control (Fig. 2A, B).

EA induces cytoplasmic distribution of TDP-43

Immunocytochemistry showed that endogenous TDP-43 disappeared from the nucleus, translocated to the cytoplasm, and became phosphorylated at least in some population of NSC34 cells treated with 70 μM EA for 5 h, whereas this protein was localized in the nucleus and was not phosphorylated in untreated cells (Fig. 3A). Although the majority of cytoplasmic TDP-43 was diffusely distributed under EA treatment, it was also localized in stress granules (SGs), which were labeled with TIAR (Fig. 3A). The time lapse analysis of NSC43 cells expressing GFP-WT-TDP-43 demonstrated cytoplasmic distribution of TDP-43 in the majority of the cells treated with 70 μM EA, but TDP-43 consistently localized in the nucleus of cells co-treated with 2 mM NAC (Fig. 3B, C).

H_2O_2 induces C-terminal phosphorylation, C-terminal fragmentation, insolubilization, and cytoplasmic distribution of TDP-43

To confirm that the TDP-43 modifications are not induced by the specific toxicity of EA, we investigated the effects of H_2O_2, another

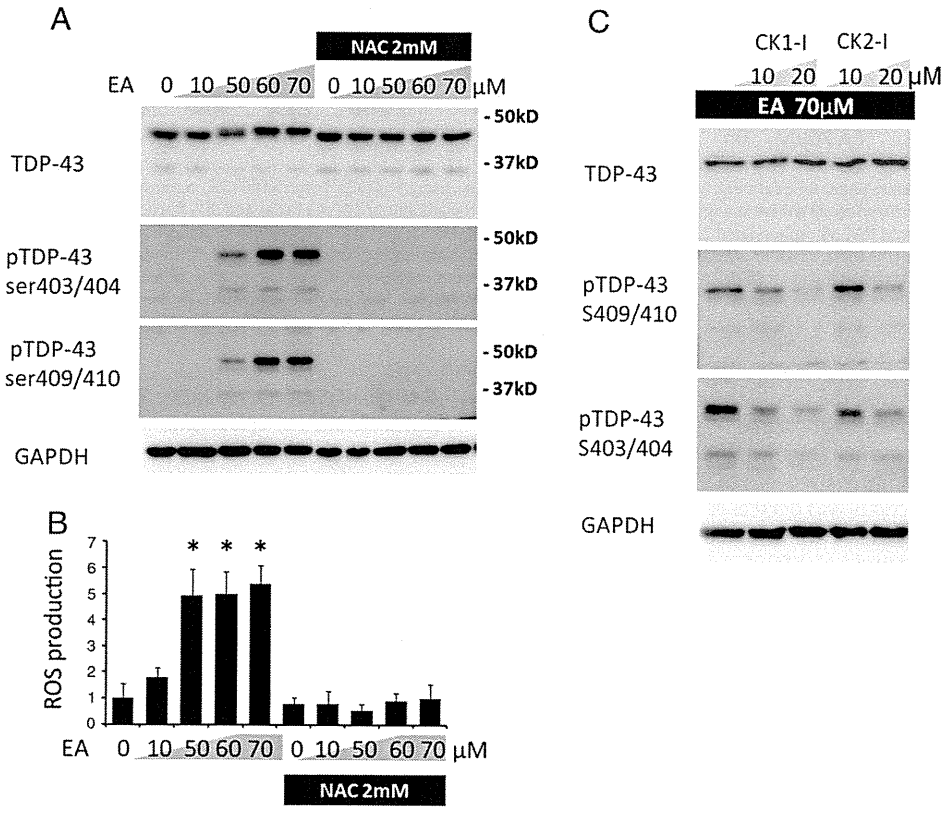

Fig. 1. TDP-43 phosphorylation induced by EA. (A) Immunoblots of NSC34 cells. EA induced TDP-43 C-terminal phosphorylation at S403/404 and S409/410 in a dose-dependent manner. The phosphorylation was prevented by 2 mM NAC. (B) Quantification of ROS by CM-H2DCFDA oxidative assay. The values relative to those of controls are shown. ROS production was increased by EA induction and suppressed by 2 mM NAC. Asterisk denotes significant difference from control ($p<0.0001$, $n=6$). Error bars indicate SD. (C) Immunoblots of NSC34 cells treated with 70 μM of EA. Casein kinase 1 and 2 inhibitors (CK1-I and CK2-I) both prevented the phosphorylation of TDP-43 in a dose-dependent manner.

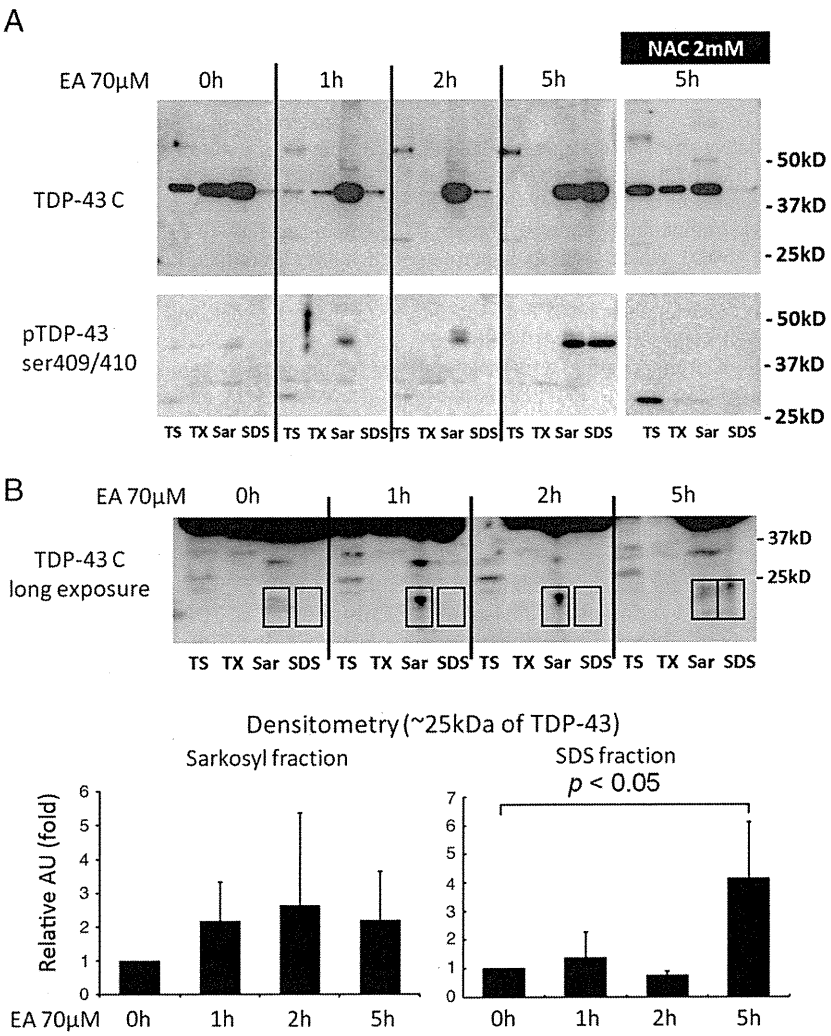

Fig. 2. Analysis of TDP-43 solubility under EA treatment. (A) Sequential extraction analysis using Tris (TS), Triton X100 (TX), Sarkosyl (Sar), and SDS buffers. The amount of TDP-43 in TS and TX fractions was decreased by 70 μM EA in a time-dependent manner, while the amount of TDP-43 in Sar and SDS fractions was increased by the treatment. These phenomena were prevented by 2 mM NAC. Phosphorylated TDP-43 (S409/410) was increased in Sar and SDS fractions in a time-dependent manner. (B) Densitometric quantitation of TDP-43C-terminal fragment (CTF). The relative intensities to controls are shown in arbitrary units (AU). Long exposure of immunoblots with anti-TDP-43 antibody (405–414) (TDP-43C) showed ~25 kDa C-terminal fragment (CTF) in Sar and SDS fractions. The amount of TDP-43 CTF was significantly increased in the SDS fraction at 5 h after EA induction (n = 3). Error bars indicate SD.

inducer of oxidative stress, on the modifications of TDP-43. Immunoblots of NSC34 cells showed that 10 mM H_2O_2 induced C-terminal phosphorylation and C-terminal fragmentation of TDP-43 (Fig. S4A). In the sequential extraction analysis of NSC34 cells, the amount of TDP-43 in TS and TX fractions was decreased by 10 mM H_2O_2, while that of TDP-43 in SDS fraction was increased by the treatment (Fig. S4B). The time lapse analysis of NSC34 cells expressing GFP-WT-TDP-43 showed that 10 mM H_2O_2 induced cytoplasmic distribution of TDP-43 (Fig. S4C).

EA induces C-terminal phosphorylation and cytoplasmic distribution of TDP-43 in primary cortical neurons

To investigate the effect of oxidative stress in neurons, 5-day in vivo (5 DIV) mouse primary cortical neurons were treated with EA for 5 h. Immunoblots showed that EA induced TDP-43 phosphorylation at S403/404 and S409/410 in a dose-dependent manner, and 2 mM NAC prevented the phosphorylation (Fig. 4A). In the time lapse analysis of neurons expressing GFP-WT-TDP-43, TDP-43 was distributed in the cytoplasm in the presence of 30 μM EA (Fig. 4B).

C-terminal phosphorylation of TDP-43 is not mandatory for its insolubilization or cytoplasmic distribution under EA

Since C-terminal phosphorylation of TDP-43 was accompanied by insolubilization and distribution to the cytoplasm in response to oxidative stress, we investigated the effect of C-terminal phosphorylation of TDP-43 using a nonphosphorylable TDP-43 (SA-TDP-43) mutant which contains serine to alanine substitutions at 403/404 and 409/410 (Fig. 5A). We used N-terminal tagged TDP-43, since C-terminal tagged TDP-43 was not detected by anti-pTDP-43 antibody in the immunoblots even under conditions of oxidative stress sufficient to phosphorylate endogenous TDP-43 (Fig. S1). As was seen with WT-TDP-43 under normal conditions, GFP-tagged and V5-tagged SA-TDP-43 were located in the nucleus (Fig. S2). In the immunoblots, endogenous and GFP-WT-TDP-43 were phosphorylated in the presence of 70 μM EA, but GFP-SA-TDP-43 was not phosphorylated even at an EA concentration of 70 μM (Fig. 5B). The time lapse analysis of NSC34 cells demonstrated that GFP-SA-TDP-43 translocated to the cytoplasm (Fig. 6A). The proportion of the cells with cytoplasmic distribution of TDP-43 under oxidative stress was not

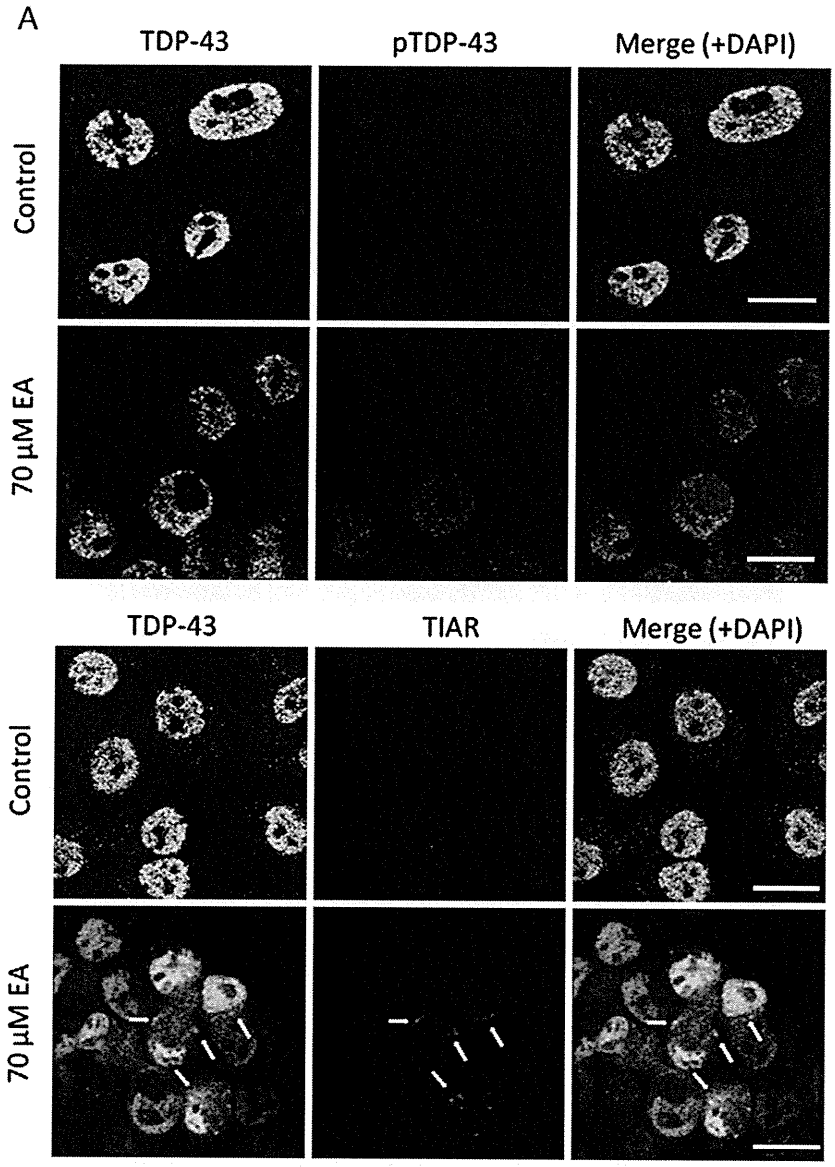

Fig. 3. Cytoplasmic distribution of TDP-43 induced by EA. (A) Immunocytochemistry of NSC34 cells. Cells were stained with anti-TDP-43 antibody (green), anti-phospho-specific TDP-43 (pTDP-43) (S409/410) or anti-TIAR antibody (red), and DAPI (blue). EA treatment (70 μM, 5 h) induced translocation of TDP-43 from the nucleus to the cytoplasm in NSC34 cells. Cytoplasmic TDP-43 was immunopositive for pTDP-43 antibody. In the control cells TDP-43 localized in the nucleus without phosphorylation. TDP-43 co-localized with stress granule marker, TIAR under EA treatment, although the majority of cytoplasmic TDP-43 was diffusely distributed. Arrows indicate stress granules. Scale bars represent 10 μm. (B) Time lapse analysis of NSC43 cells expressing GFP-WT-TDP-43. GFP and phase contrast images showed that TDP-43 was distributed to the cytoplasm when exposed to 70 μM EA, but this distribution was prevented by 2 mM of NAC. (C) The proportion of cells with cytoplasmic distribution of TDP-43 (cells with cyto-TDP) in the GFP-TDP-43 expressing cells 0 h or 5 h after EA induction without or with NAC treatment. Three areas per sample were measured. Error bars indicate SD.

different between WT- and SA-TDP-43 (Fig. 6B). Sequential extraction of NSC34 cells was performed using V5-tagged TDP-43 vectors, since the Sar-insoluble fraction of GFP-TDP-43 was abundant even in the absence of oxidative stress (data not shown). The amount of Sar-insoluble fraction of SA-TDP-43 detected was the same as was seen with WT-TDP-43. (Fig. 7A, B). These findings indicate that phosphorylation is not necessary for oxidative-stress mediated insolubilization and cytoplasmic distribution of TDP-43. Next, we performed MTS assay of NSC34 cells to investigate the effect of TDP-43 and its modifications on the cell viability. The results showed that no significant difference in the viability among the cells expressing GFP-mock, GFP-WT- and GFP-SA-TDP-43, either 0 h or 5 h after EA induction (Fig. S3).

Discussion

Post-translational modifications of TDP-43 such as C-terminal phosphorylation, insolubilization, C-terminal fragmentation, and cytoplasmic distribution are pathological hallmarks of TDP-43 proteinopathies (Arai et al., 2006; Hasegawa et al., 2008; Neumann et al., 2006). TDP-43 with defective nuclear localization signal (NLS) was shown to promote cytoplasmic aggregation, C-terminal phosphorylation, and C-terminal fragmentation of TDP-43 in cell-based studies (Nonaka et al., 2009a; Winton et al., 2008). In addition, overexpression of TDP-43 CTF lead to phosphorylation and formation of cytoplasmic aggregates (Igaz et al., 2009; Nonaka et al., 2009b). Although these observations suggest that the cytoplasmic localization

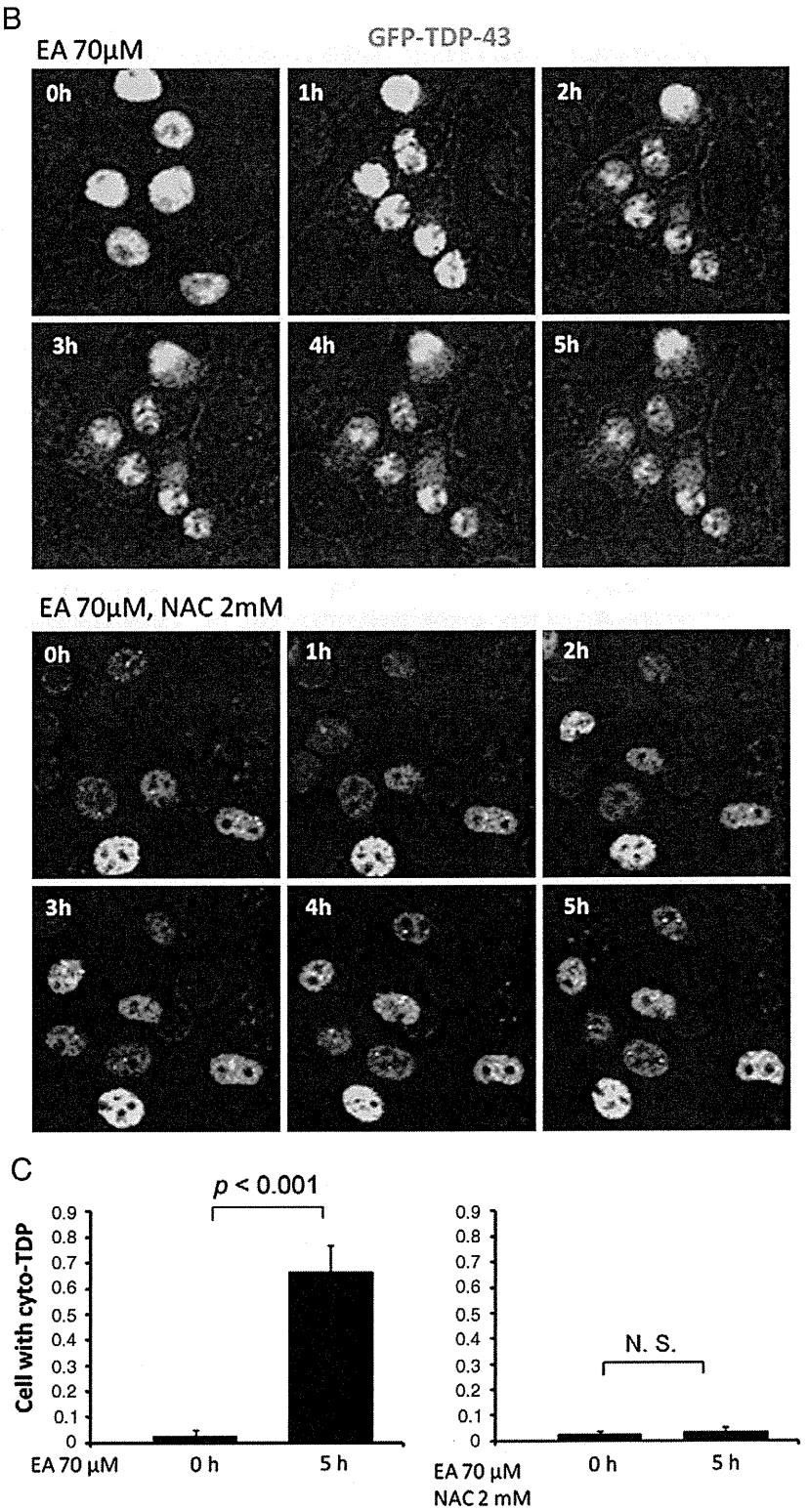

Fig. 3 (*continued*).

or fragmentation of TDP-43 facilitates its pathological modification such as aggregation and phosphorylation, the initial cause of these modifications in TDP-43 proteinopathies has not been fully elucidated. Some studies have demonstrated that artificial axonal damage induces transient cytoplasmic distribution of TDP-43 in motor neurons (Moisse et al., 2009; Sato et al., 2009), indicating that the pathological distribution of TDP-43 may result from the cellular response to neuronal injury or axonal obstruction. However, in these affected neurons, aggregation, C-terminal fragmentation and phosphorylation of TDP-43 were not observed. Furthermore, zinc-induced nuclear

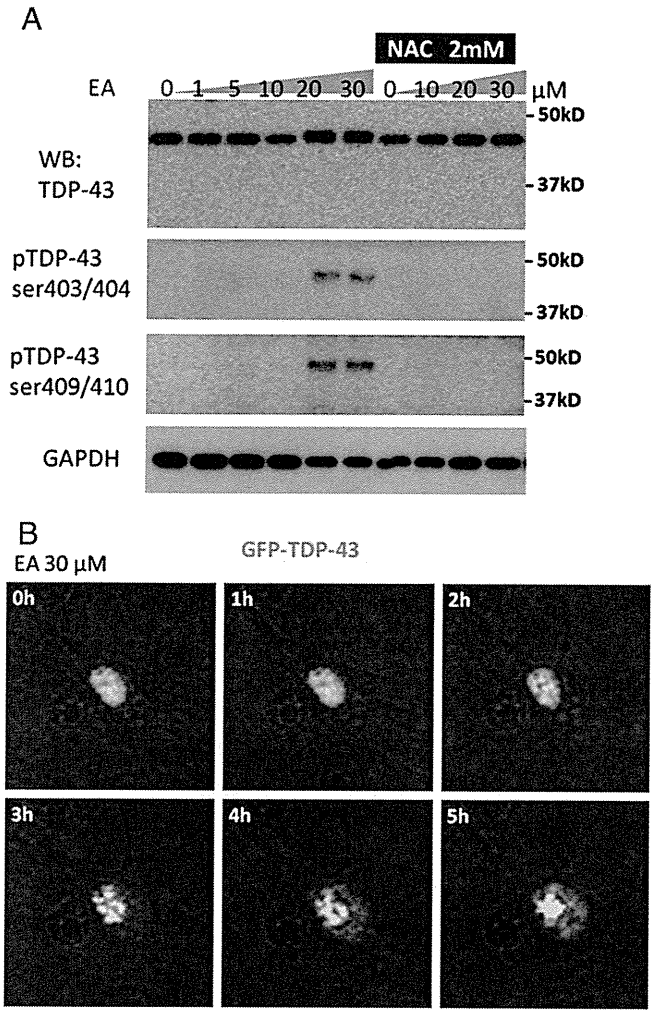

Fig. 4. TDP-43 modification induced by EA in primary cortical neuron. (A) Immunoblots of primary cortical neurons. EA induced TDP-43 phosphorylation at S403/404 and S409/410 in a dose-dependent manner, and this was prevented by 2 mM NAC. (B) Time lapse analysis of neurons expressing GFP-WT-TDP-43. TDP-43 in primary cultures was distributed to the cytoplasm in the presence of 30 μM EA.

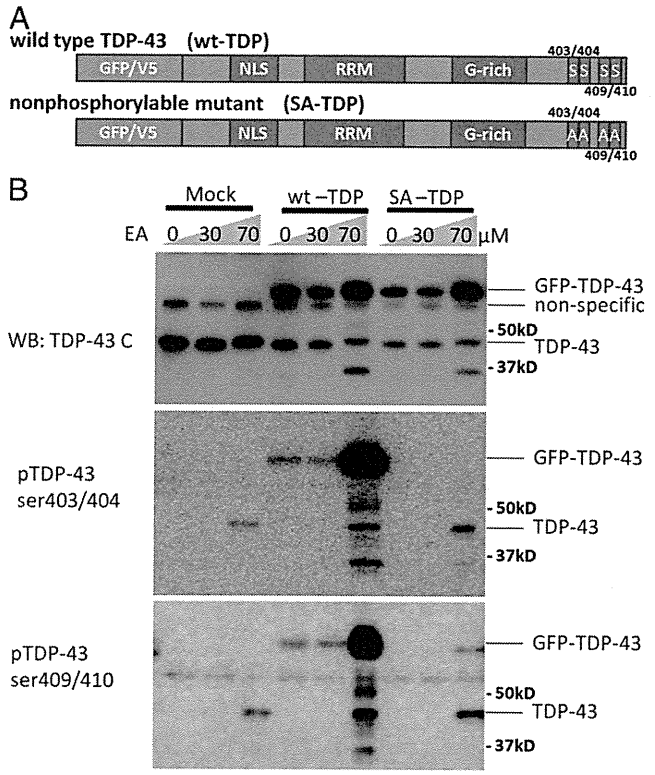

Fig. 5. Nonphosphorylable mutant of TDP-43. (A) Structures of WT- and SA-TDP-43 vectors. SA-TDP-43 contains serine to alanine substitutions at 403/404 and 409/410. (B) Immunoblots of NSC34 cells expressing GFP-WT- or GFP-SA-TDP-43. Endogenous and GFP-WT-TDP-43 were phosphorylated at both 403/404 and 409/410 by 70 μM EA, but GFP-SA-TDP-43 was not phosphorylated by the treatment.

inclusion formations have also been observed in SY5Y cells, but not C-terminal fragmentation or phosphorylation of TDP-43 (Caragounis et al., 2010).

In the present study, we demonstrated that a compound that induces cellular glutathione depletion, EA induced C-terminal phosphorylation of TPD-43 at S403/404 and S409/410 in NSC34 cells and mouse primary cortical neurons, and that NAC completely prevented this phosphorylation. In addition, inhibitors of both CK1 and CK2 also prevented the phosphorylation in a dose-dependent manner. These findings indicate that C-terminal phosphorylation of TDP-43 occurs as a consequence of oxidative stress induced by glutathione depletion and is mediated by CK1 and CK2. Furthermore, the sequential extract analysis showed that EA reduced the solubility of TDP43 and increased the amount of ~25 kDa CTF in the Sar-insoluble fraction. Additionally, EA also induced cytoplasmic distribution of TDP-43 in NSC34 cells and primary cortical neurons. The time lapse analysis showed that cytoplasmic distribution of TDP-43 was seen in the majority of NSC34 cells. Although the immunocytochemistry of TDP-43 demonstrated that cytoplasmic distribution of TDP-43 were observed only in a certain population of NSC34 cells treated with EA, this is likely due to the fact that most of damaged cells could not stay adherent to the plate during the fixation. Previous reports indicated that severe level of oxidative stress may result in apoptotic cell death, and that caspase activation induces C-terminal fragmentation of TDP-43 (Dormann et al., 2009; Zhang et al., 2007). These observations do not exclude the possibility that caspase activation contributes to TDP-43 modifications that were observed under EA treatment. The results of the present study demonstrated that H_2O_2, another inducer of oxidative stress, also causes C-terminal phosphorylation, fragmentation, insolubilization, and cytoplasmic distribution of TDP-43 as observed under EA exposure. These data suggest that oxidative stress is involved in the process of the pathological TDP-43 modifications seen in TDP-43 proteinopathies. The facts that oxidative stress is associated with aging-related disorders (Frederickson et al., 2005; Migliore, 2005) and that TDP-43 proteinopathies are aging process-related diseases may support our assumption that oxidative stress possibly mediates TDP-43 modification. A high frequency of abnormal TDP-43 pathology such as C-terminal phosphorylation has been found not only in patients with TDP-43 proteinopathies but also in patients with other neurodegenerative disease such as AD, DLB, and HD (Arai et al., 2010). Since numerous studies have demonstrated increased oxidative cellular damage in these conditions (Butterfield et al., 2007; Lovell and Markesbery, 2007; Nunomura et al., 2002), oxidative stress may be a cause of pathological TDP-43 modification in various neurodegenerative disorders.

Several studies demonstrated that TDP-43 is involved in SGs under cellular stresses including arsenite treatment and heat shock (Colombrita et al., 2009; Liu-Yesucevitz et al., 2010; McDonald et al., 2011; Nishimoto et al., 2010). Although TDP-43 was seen as a component of SGs under EA treatment, majority of cytoplasmic TDP-43 was independent of SGs and was diffusely distributed. These findings suggest that there is SG-independent mechanism for cytoplasmic distribution of TDP-43 under oxidative stress induced by glutathione depletion.

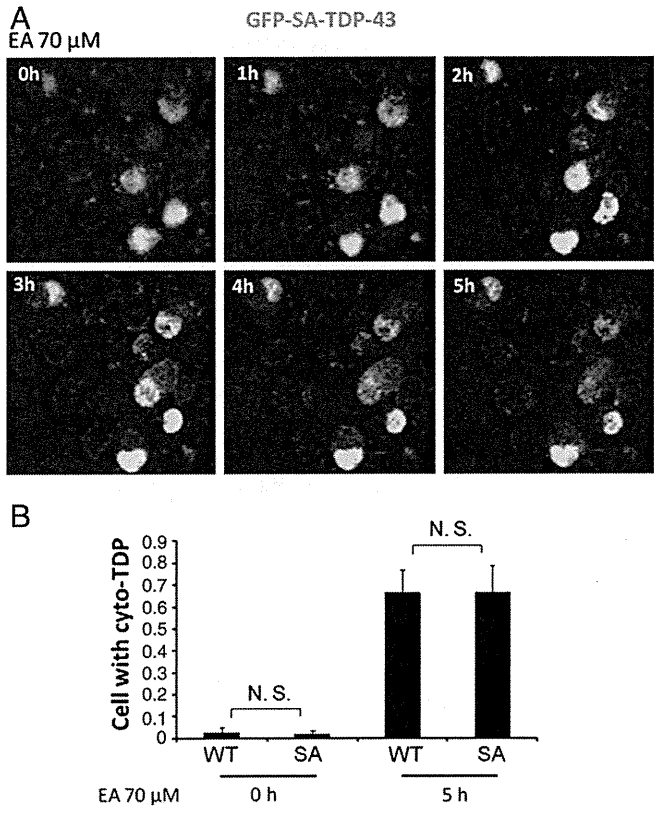

Fig. 6. The effect of C-terminal phosphorylation on TDP-43 distribution. (A) Time lapse analysis of NSC34 cells expressing GFP-SA-TDP-43. GFP-SA-TDP-43 was distributed to the cytoplasm by 70 μM of EA. (B) The proportion of cells with cytoplasmic distribution of TDP-43 (cells with cyto-TDP) in the GFP-TDP-43 expressing cells. The proportion of cells with cyto-TDP was not different between WT- and SA-TDP-43, either 0 h or 5 h after EA induction. Three areas per sample were measured. Error bars indicate SD.

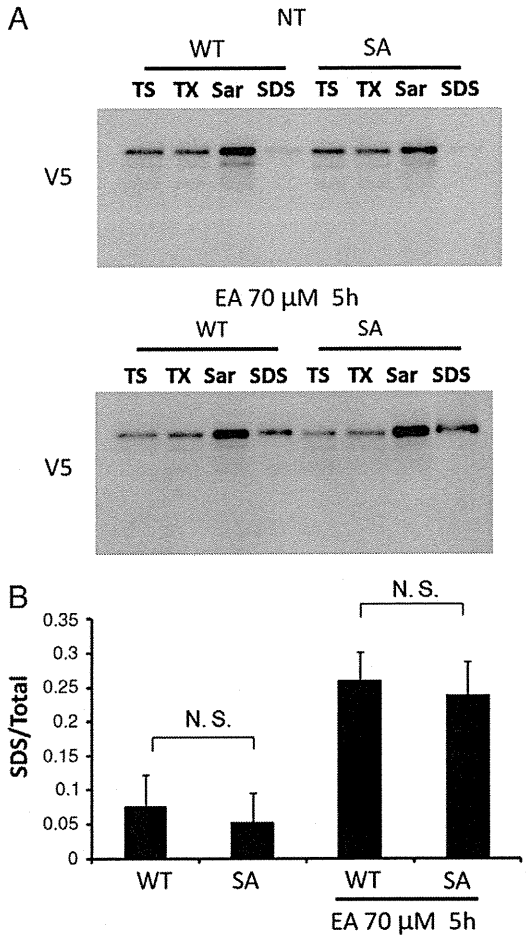

Fig. 7. The effect of C-terminal phosphorylation on TDP-43 solubility. (A) Sequential extraction of NSC34 cells expressing V5-WT- or V5-SA-TDP-43. (B) Densitometric quantitation of Sar-insoluble V5-TDP-43. Ratio of Sar-insoluble fraction from the whole fraction did not differ between WT- and SA-TDP-43 with or without 70 μM EA. Three independent experiments were performed. Error bars indicate SD.

In the present study, S403/404 and S409/410 of TDP-43 were phosphorylated together with insolubilization and cytoplasimic distribution of the protein. The hyperphosphorylation of disease marker proteins is a common feature of neurodegenerative disorders, and its relation to the pathogenesis has been intensively investigated: Tau in AD; huntingtin in HD; and alfa-synuclein in PD and DLB (Ballatore et al., 2007; Fujiwara et al., 2002; Gu et al., 2009). A number of studies have demonstrated that disease-specific phosphorylation of these marker proteins modulates aggregation and potentially influences disease pathogenesis (Azeredo da Silveira et al., 2009; Gu et al., 2009). In the present study, there was no difference between wild type and non-phosphorylable TDP-43 in the degree of insolubilization and cytoplasmic translocation under oxidative stress conditions, suggesting that C-terminal phosphorylation of TDP-43 is not mandatory for aggregation or abnormal intracellular distribution. In support with our findings, there is a study demonstrating that C-terminal phosphorylation of TDP-43 is not substantially required for the cytoplasmic aggregation (Brady et al., 2010). In addition, our results show that C-terminal tags interfere with the detection of TDP-43 phosphorylation, providing a cautionary note for cell-based and animal studies of TDP-43 with a C-terminal tag.

We further examined whether the pathological modifications of TDP-43 contribute to cell vulnerability to glutathione depletion. In the analysis of MTS assay, the viabilities of NSC34 cells were decreased by EA treatment. Although GFP-WT-TDP-43 was fully phosphorylated, insolubilized and distributed to cytoplasm in the cells treated with EA, there was no significant difference in the viability between the cells expressing GFP-mock and GFP-WT-TDP-43. In addition, the viability of NSC34 cells expressing GFP-SA-TDP-43 was not different from that of the cells expressing GFP-WT-TDP-43. These findings suggest that TDP-43 modification may not affect cell viability under oxidative stress induced by glutathione depletion.

In conclusion, we demonstrated that oxidative stress induced by glutathione depletion instigated TDP-43 modifications including C-terminal phosphorylation, insolubilization, C-terminal fragmentation and cytoplasmic distribution, and that these changes reproduce the pathological features of TDP-43 proteinopathies and other neurodegenerative diseases such as AD.

Supplementary materials related to this article can be found online at doi:10.1016/j.nbd.2011.12.002.

Funding

Funding: This work was supported by a Center-of-Excellence (COE) grant, a Grant-in-Aid for Scientific Research on Innovated Areas "Foundation of Synapse and Neurocircuit Pathology," and Grant-in-Aids from Ministry of Education, Culture, Sports, Science, and Technology of Japan; grants from the Ministry of Health, Labor and Welfare of Japan; and Core Research for Evolutional Science and Technology (CREST) of the Japan Science and Technology Agency (JST).

References

Abe, K., et al., 1995. Induction of nitrotyrosine-like immunoreactivity in the lower motor neuron of amyotrophic lateral sclerosis. Neurosci. Lett. 199, 152–154.

Abe, K., et al., 1997. Upregulation of protein-tyrosine nitration in the anterior horn cells of amyotrophic lateral sclerosis. Neurol. Res. 19, 124–128.
Amador-Ortiz, C., et al., 2007. TDP-43 immunoreactivity in hippocampal sclerosis and Alzheimer's disease. Ann. Neurol. 61, 435–445.
Arai, T., et al., 2006. TDP-43 is a component of ubiquitin-positive tau-negative inclusions in frontotemporal lobar degeneration and amyotrophic lateral sclerosis. Biochem. Biophys. Res. Commun. 351, 602–611.
Arai, T., et al., 2009. Phosphorylated TDP-43 in Alzheimer's disease and dementia with Lewy bodies. Acta Neuropathol. 117, 125–136.
Arai, T., et al., 2010. Phosphorylated and cleaved TDP-43 in ALS, FTLD and other neurodegenerative disorders and in cellular models of TDP-43 proteinopathy. Neuropathology 30, 170–181.
Ayala, Y.M., et al., 2005. Human, Drosophila, and C.elegans TDP43: nucleic acid binding properties and splicing regulatory function. J. Mol. Biol. 348, 575–588.
Ayala, Y.M., et al., 2008. TDP-43 regulates retinoblastoma protein phosphorylation through the repression of cyclin-dependent kinase 6 expression. Proc. Natl. Acad. Sci. U. S. A. 105, 3785–3789.
Azeredo da Silveira, S., et al., 2009. Phosphorylation does not prompt, nor prevent, the formation of alpha-synuclein toxic species in a rat model of Parkinson's disease. Hum. Mol. Genet. 18, 872–887.
Ballatore, C., et al., 2007. Tau-mediated neurodegeneration in Alzheimer's disease and related disorders. Nat. Rev. Neurosci. 8, 663–672.
Beal, M.F., et al., 1997. Increased 3-nitrotyrosine in both sporadic and familial amyotrophic lateral sclerosis. Ann. Neurol. 42, 644–654.
Brady, O.A., et al., 2010. Regulation of TDP-43 aggregation by phosphorylation and p62/SQSTM1. J. Neurochem. 116, 248–259.
Buratti, E., et al., 2005. TDP-43 binds heterogeneous nuclear ribonucleoprotein A/B through its C-terminal tail: an important region for the inhibition of cystic fibrosis transmembrane conductance regulator exon 9 splicing. J. Biol. Chem. 280, 37572–37584.
Buratti, E., et al., 2010. Nuclear factor TDP-43 can affect selected microRNA levels. FEBS J. 277, 2268–2281.
Butterfield, D.A., et al., 2007. Roles of amyloid beta-peptide-associated oxidative stress and brain protein modifications in the pathogenesis of Alzheimer's disease and mild cognitive impairment. Free Radic. Biol. Med. 43, 658–677.
Caragounis, A., et al., 2010. Zinc induces depletion and aggregation of endogenous TDP-43. Free Radic. Biol. Med. 48, 1152–1161.
Colombrita, C., et al., 2009. TDP-43 is recruited to stress granules in conditions of oxidative insult. J. Neurochem. 111, 1051–1061.
Dormann, D., et al., 2009. Proteolytic processing of TAR DNA binding protein-43 by caspases produces C-terminal fragments with disease defining properties independent of progranulin. J. Neurochem. 110, 1082–1094.
Ferrante, R.J., et al., 1997. Evidence of increased oxidative damage in both sporadic and familial amyotrophic lateral sclerosis. J. Neurochem. 69, 2064–2074.
Frederickson, C.J., et al., 2005. The neurobiology of zinc in health and disease. Nat. Rev. Neurosci. 6, 449–462.
Fujiwara, H., et al., 2002. alpha-Synuclein is phosphorylated in synucleinopathy lesions. Nat. Cell Biol. 4, 160–164.
Geser, F., et al., 2008. Pathological TDP-43 in parkinsonism-dementia complex and amyotrophic lateral sclerosis of Guam. Acta Neuropathol. 115, 133–145.
Gu, X., et al., 2009. Serines 13 and 16 are critical determinants of full-length human mutant huntingtin induced disease pathogenesis in HD mice. Neuron 64, 828–840.
Hasegawa, M., et al., 2007. TDP-43 is deposited in the Guam parkinsonism-dementia complex brains. Brain 130, 1386–1394.
Hasegawa, M., et al., 2008. Phosphorylated TDP-43 in frontotemporal lobar degeneration and amyotrophic lateral sclerosis. Ann. Neurol. 64, 60–70.
Igaz, L.M., et al., 2009. Expression of TDP-43 C-terminal Fragments in Vitro Recapitulates Pathological Features of TDP-43 Proteinopathies. J. Biol. Chem. 284, 8516–8524.
Iguchi, Y., et al., 2009. TDP-43 depletion induces neuronal cell damage through dysregulation of Rho family GTPases. J. Biol. Chem. 284, 22059–22066.
Keelan, J., et al., 2001. Quantitative imaging of glutathione in hippocampal neurons and glia in culture using monochlorobimane. J. Neurosci. Res. 66, 873–884.
Liu-Yesucevitz, L., et al., 2010. Tar DNA binding protein-43 (TDP-43) associates with stress granules: analysis of cultured cells and pathological brain tissue. PLoS One 5, e13250.
Lovell, M.A., Markesbery, W.R., 2007. Oxidative DNA damage in mild cognitive impairment and late-stage Alzheimer's disease. Nucleic Acids Res. 35, 7497–7504.
McDonald, K.K., et al., 2011. TAR DNA-binding protein 43 (TDP-43) regulates stress granule dynamics via differential regulation of G3BP and TIA-1. Hum. Mol. Genet. 20, 1400–1410.
Migliore, L., 2005. Searching for the role and the most suitable biomarkers of oxidative stress in Alzheimer's disease and in other neurodegenerative diseases. Neurobiol. Aging 26, 587–595.
Moisse, K., et al., 2009. Divergent patterns of cytosolic TDP-43 and neuronal progranulin expression following axotomy: implications for TDP-43 in the physiological response to neuronal injury. Brain Res. 1249, 202–211.
Neumann, M., et al., 2006. Ubiquitinated TDP-43 in frontotemporal lobar degeneration and amyotrophic lateral sclerosis. Science 314, 130–133.
Nishimoto, Y., et al., 2010. Characterization of alternative isoforms and inclusion body of the TAR DNA-binding protein-43. J. Biol. Chem. 285, 608–619.
Nonaka, T., et al., 2009a. Phosphorylated and ubiquitinated TDP-43 pathological inclusions in ALS and FTLD-U are recapitulated in SH-SY5Y cells. FEBS Lett. 583, 394–400.
Nonaka, T., et al., 2009b. Truncation and pathogenic mutations facilitate the formation of intracellular aggregates of TDP-43. Hum. Mol. Genet. 18, 3353–3364.
Nunomura, A., et al., 2002. Neuronal RNA oxidation is a prominent feature of dementia with Lewy bodies. Neuroreport 13, 2035–2039.
Polymenidou, M., et al., 2011. Long pre-mRNA depletion and RNA missplicing contribute to neuronal vulnerability from loss of TDP-43. Nat. Neurosci. 14, 459–468.
Rizzardini, M., et al., 2003. Mitochondrial dysfunction and death in motor neurons exposed to the glutathione-depleting agent ethacrynic acid. J. Neurol. Sci. 207, 51–58.
Sato, T., et al., 2009. Axonal ligation induces transient redistribution of TDP-43 in brainstem motor neurons. Neuroscience 164, 1565–1578.
Sephton, C.F., et al., 2011. Identification of neuronal RNA targets of TDP-43-containing ribonucleoprotein complexes. J. Biol. Chem. 286, 1204–1215.
Shaw, I.C., et al., 1995. Studies on cellular free radical protection mechanisms in the anterior horn from patients with amyotrophic lateral sclerosis. Neurodegeneration 4, 391–396.
Strong, M.J., et al., 2007. TDP43 is a human low molecular weight neurofilament (hNFL) mRNA-binding protein. Mol. Cell. Neurosci. 35, 320–327.
Tollervey, J.R., et al., 2011. Characterizing the RNA targets and position-dependent splicing regulation by TDP-43. Nat. Neurosci. 14, 452–458.
Wang, I.F., et al., 2002. Higher order arrangement of the eukaryotic nuclear bodies. Proc. Natl. Acad. Sci. U. S. A. 99, 13583–13588.
Wang, H.Y., et al., 2004. Structural diversity and functional implications of the eukaryotic TDP gene family. Genomics 83, 130–139.
Winton, M.J., et al., 2008. Disturbance of nuclear and cytoplasmic TAR DNA-binding protein (TDP-43) induces disease-like redistribution, sequestration, and aggregate formation. J. Biol. Chem. 283, 13302–13309.
Zhang, Y.J., et al., 2007. Progranulin mediates caspase-dependent cleavage of TAR DNA binding protein-43. J. Neurosci. 27, 10530–10534.

Neurobiology of Disease 41 (2011) 111–118

Contents lists available at ScienceDirect

Neurobiology of Disease

journal homepage: www.elsevier.com/locate/ynbdi

Mitochondrial membrane potential decrease caused by loss of PINK1 is not due to proton leak, but to respiratory chain defects

Taku Amo [a,1], Shigeto Sato [b], Shinji Saiki [b], Alexander M. Wolf [a], Masaaki Toyomizu [c], Clement A. Gautier [d], Jie Shen [d], Shigeo Ohta [a], Nobutaka Hattori [b,*]

[a] Department of Biochemistry and Cell Biology, Institute of Development and Aging Sciences, Graduate School of Medicine, Nippon Medical School, 1-396 Kosugi-cho, Nakahara-ku, Kawasaki 211-8533, Japan
[b] Department of Neurology, Juntendo University School of Medicine, 2-1-1 Hongo, Bunkyo-ku, Tokyo 113-8421, Japan
[c] Animal Nutrition, Life Sciences, Graduate School of Agricultural Science, Tohoku University, 1-1 Tsutsumidori-Amamiyamachi, Aoba-ku, Sendai 981-8555, Japan
[d] Center for Neurologic Diseases, Brigham and Women's Hospital, Program in Neuroscience, Harvard Medical School, Boston, MA 02115, USA

ARTICLE INFO

Article history:
Received 29 June 2010
Revised 17 August 2010
Accepted 25 August 2010
Available online 15 September 2010

Keywords:
Parkinson's disease
Mitochondria
PINK1
Parkin
Membrane potential
Oxidative phosphorylation
Modular kinetic analysis
Proton leak
Reactive oxygen species

ABSTRACT

Mutations in *PTEN-induced putative kinase 1* (*PINK1*) cause a recessive form of Parkinson's disease (PD). PINK1 is associated with mitochondrial quality control and its partial knock-down induces mitochondrial dysfunction including decreased membrane potential and increased vulnerability against mitochondrial toxins, but the exact function of PINK1 in mitochondria has not been investigated using cells with null expression of PINK1. Here, we show that loss of PINK1 caused mitochondrial dysfunction. In PINK1-deficient ($PINK1^{-/-}$) mouse embryonic fibroblasts (MEFs), mitochondrial membrane potential and cellular ATP levels were decreased compared with those in littermate wild-type MEFs. However, mitochondrial proton leak, which reduces membrane potential in the absence of ATP synthesis, was not altered by loss of PINK1. Instead, activity of the respiratory chain, which produces the membrane potential by oxidizing substrates using oxygen, declined. H_2O_2 production rate by $PINK1^{-/-}$ mitochondria was lower than $PINK1^{+/+}$ mitochondria as a consequence of decreased oxygen consumption rate, while the proportion (H_2O_2 production rate per oxygen consumption rate) was higher. These results suggest that mitochondrial dysfunctions in PD pathogenesis are caused not by proton leak, but by respiratory chain defects.

Introduction

Parkinson's disease (PD) is a neurodegenerative disease characterized by loss of dopaminergic neurons in the substantia nigra. Mitochondrial dysfunction has been proposed as a major factor in the pathogenesis of sporadic and familial PD (Abou-Sleiman et al., 2006). In particular, the identification of mutations in *PTEN-induced putative kinase 1* (*PINK1*) has strongly implicated mitochondrial dysfunction owing to its loss of function in the pathogenesis of PD (Valente et al., 2004). PINK1 contains an N-terminal mitochondrial targeting sequence (MTS) and a serine/threonine kinase domain (Valente et al., 2004). PINK1 kinase activity is crucial for mitochondrial maintenance via TRAP phosphorylation (Pridgeon et al., 2007). Loss of PINK1 function induces increased vulnerability to various stresses (Exner et al., 2007; Haque et al., 2008; Pridgeon et al., 2007; Wood-Kaczmar et al., 2008). However, silencing of PINK1 has only been partial and only one study has been performed to assess mitochondrial functions in steady and artificial states with complete ablation of PINK1 expression (Gautier et al., 2008).

Several studies have shown that PINK1 acts upstream of parkin in the same genetic pathway (Clark et al., 2006; Park et al., 2006) and co-overexpressed PINK1 and parkin both co-localized to mitochondria (Kim et al., 2008). Overexpression of PINK1 promotes mitochondrial fission (Yang et al., 2008). Fission followed by selective fusion segregates dysfunctional mitochondria and permits their removal by autophagy (Twig et al., 2008). PINK1 loss-of-function decreases mitochondrial membrane potential (Chu, 2010) and the PINK1–parkin pathway is associated with mitochondrial elimination in cultured cells treated with the mitochondrial uncoupler carbonyl cyanide *m*-chlorophenylhydrazone (CCCP), which causes mitochondrial depolarization (Geisler et al., 2010; Kawajiri et al., 2010; Matsuda et al., 2010; Narendra et al., 2008, 2010; Vives-Bauza et al., 2010). However, the exact mechanism underlying the mitochondrial depolarization induced by PINK1 defects leading to mitochondrial autophagy has not been examined in detail.

Abbreviations: $\Delta\psi$, mitochondrial membrane potential; FCCP, carbonyl cyanide *p*-trifluoromethoxyphenylhydrazone; MEFs, mouse embryonic fibroblasts; PD, Parkinson's disease; PINK1, PTEN-induced putative kinase 1; ROS, reactive oxygen species; TMRM, tetramethylrhodamine methyl ester; TPMP, triphenylmethylphosphonium.

* Corresponding author. Fax: +81 3 5800 0547.
E-mail address: nhattori@juntendo.ac.jp (N. Hattori).
[1] Present address: Department of Applied Chemistry, National Defense Academy, 1-10-20 Hashirimizu, Yokosuka 239-8686, Japan.

Available online on ScienceDirect (www.sciencedirect.com).

0969-9961/$ – see front matter © 2010 Elsevier Inc. All rights reserved.
doi:10.1016/j.nbd.2010.08.027

Here, we describe a detailed characterization of mitochondria in PINK1-deficient cells. We show that PINK1 deficiency causes a decrease in mitochondrial membrane potential, which is not due to proton leak, but to respiratory chain defects.

Materials and methods

PINK1 knock-out mouse embryonic fibroblasts (MEFs)

PINK1 knock-out MEFs were prepared and cultured as described previously (Matsuda et al., 2010). Mouse embryonic fibroblasts (MEFs) were derived from E12.5 embryos containing littermate 4 mice of each genotype. Embryos were mechanically dispersed by repeated passage through a P1000 pipette tip and plated with MEF media containing DME, 10% FCS, 1× nonessential amino acids, 1 mM L-glutamine, penicillin/streptomycin (invitrogen). The $\psi 2$ cell line, an ecotropic retrovirus packaging cell line, was maintained in Dulbecco's modified Eagle medium (DMEM, Sigma) with 5% fetal bovine serum and 50 μg/ml kanamicin. Transfection of the $\psi 2$ cells with pMESVTS plasmids containing an SV40 large T antigen was performed by lipofection method according to the manual provided by the manufacturer (GIBCO BRL). Five micrograms of the plasmids was used for each transfection. Transfectants were selected by G418 at the concentration of 0.5 mg/ml, and 10 clonal cell lines were established. The highest titer of 5×10^4 cfu/ml was obtained for the conditioned medium of a cell line designated ψ2SVTS1. 10^6 MEFs were plated onto a 10-cm culture dish and kept at 33 °C for 48 hours. Then medium was replaced with 2 ml supplemented with polybrene-supplemented medium conditioned by the ψ2SVTS1 cells at confluency for 3 days. Infection was continued for 3 hours, and the medium was replaced with a fresh one. The infected MEFs were cultured at 33 °C until immortalized cells were obtained.

We confirmed that the differences we detected in this study were due to the PINK1 deficiency, not to artificial effects by immortalization, by measuring cellular respiration rates of not immortalized MEFs from other littermates (Supplemental figure). The respiration rates of not immortalized MEFs were slightly slower than those of immortalized MEFs, but the differences between PINK1$^{+/+}$ and $^{-/-}$ MEFs were consistent (Fig. 2A).

Cell growth

Cells were seeded in 12-well plates at density of $3\sim6\times10^3$ cells/well and incubated in DMEM high glucose medium (4.5 g/l glucose and 1 mM sodium pyruvate) supplemented with 10% fetal bovine serum. After a day, the medium was replaced with DMEM glucose-free medium supplemented with 1 g/l galactose, 1 mM sodium pyruvate and 10% fetal bovine serum (DMEM galactose medium) at 37 °C in an incubator with a humidified atmosphere of 5% CO_2. Cells were trypsinized and live cells were assessed by trypan blue dye exclusion.

Mitochondrial morphological changes

Cells were seeded in 6-well plates at 2.0×10^5/well and incubated in DMEM high glucose medium (4.5 g/l glucose and 1 mM sodium pyruvate) supplemented with 10% fetal bovine serum and 1% penicillin/streptomycin. After a day, the medium was replaced with DMEM glucose-free medium supplemented with 1 g/l galactose, 1 mM sodium pyruvate and 10% fetal bovine serum (DMEM galactose medium) at 37 °C in an incubator with a humidified atmosphere of 5% CO_2. 24 hours later, cells were fixed and immunostained with anti-Tom20 antibody to visualize mitochondria according to a protocol as previously described (Kawajiri et al., 2010). All images were obtained using an Axioplan 2 imaging microscope (Carl Zeiss, Oberkochen, Germany).

Cellular ATP levels

Intracellular ATP levels were determined by a cellular ATP assay kit (TOYO B-Net, Tokyo, Japan) according to the manufacturer's instructions using a Lumat LB9507 luminometer (Berthold Technology, Bad Wildbad, Germany).

Membrane potential

Fluorescence images were recorded using a multi-dimensional imaging workstation (AS MDW, Leica Microsystems, Wetzlar, Germany) with a climate chamber maintained at 37 °C. Fluorescence was quantified with a CCD camera (CoolSnap HQ, Roper Scientific, Princeton, NJ) using a 20× objective. Cells were stained for 1 hour with a non-quenching concentration (20 nM) of tetramethylrhodamine methyl ester (TMRM) in a 96-well plate. The cell-permeable cationic dye TMRM accumulates in mitochondria according to the Nernst equation. Nuclei were stained with 250 nM Hoechst 34580. Mitochondrial TMRM fluorescence was integrated in a 40-μm diameter circular area around the nucleus, and the minimum fluorescence in this area was subtracted as background fluorescence.

Cell respiration

Cell respiration was measured at 37 °C using the Oxygen Meter Model 781 and the Mitocell MT200 closed respiratory chamber (Strathkelvin Instruments, North Lanarkshire, United Kingdom). Cells were cultured in DMEM with 4.5 g/l of glucose supplemented with 10% FBS. Cells were then trypsinized and resuspended in Leibovitz's L-15 medium (Invitrogen) at density of 8.0×10^6 cells/ml. The oxygen respiration rate was measured under each of the following three conditions: basal rate (no additions); State 4 (no ATP synthesis) [after addition of 1 μg/ml oligomycin (Sigma)], uncoupled [after addition of 3 μM FCCP (carbonyl cyanide *p*-trifluoromethoxyphenylhydrazone; Sigma)] using Strathkelvin 949 Oxygen System. After sequential measurements, the endogenous respiration rate was determined by adding 1 μM rotenone + 2 μM myxothiazol.

Mitochondrial respiration and membrane potential

Mitochondria were prepared from cultured MEFs as previously described (Amo and Brand, 2007). Mitochondrial oxygen consumption with 5 mM succinate as a respiratory substrate was measured at 37 °C using a Clark electrode (Rank Brothers, Cambridge, United Kingdom) calibrated with air-saturated respiration buffer comprising 0.115 M KCl, 10 mM KH_2PO_4, 3 mM HEPES (pH 7.2), 2 mM $MgCl_2$, 1 mM EGTA and 0.3% (w/v) defatted BSA, assumed to contain 406 nmol atomic oxygen/ml (Reynafarje et al., 1985). Mitochondrial membrane potential ($\Delta\psi$) was measured simultaneously with respiratory activity using an electrode sensitive to the lipophilic cation $TPMP^+$ (triphenylmethylphosphonium) (Brand, 1995). Mitochondria were incubated at 0.5 mg/ml in the presence of 80 ng/ml nigericin (to collapse the pH gradient so that the proton motive force was expressed exclusively as $\Delta\psi$) and 2 μM rotenone (to inhibit complex I). The $TPMP^+$-sensitive electrode was calibrated with sequential additions of $TPMP^+$ up to 2 μM, then 5 mM succinate was added to initiate respiration. Experiments were terminated with 2 μM FCCP, allowing correction for any small baseline drift. $\Delta\psi$ was calculated from the distribution of $TPMP^+$ across the mitochondrial inner membrane using a binding correction factor of 0.35 mg protein/μl. Respiratory rates with 4 mM pyruvate + 1 mM malate as a substrate in State 3 (with 0.25 mM ADP) and State 4 (with 1 μg/ml oligomycin) were determined using the Oxygen Meter Model 781 and the Mitocell MT200 closed respiratory chamber (Strathkelvin Instruments).

Modular kinetic analysis

To investigate differences in oxidative phosphorylation caused by PINK1 knock-out, we applied a systems approach, namely modular kinetic analysis (Amo and Brand, 2007; Brand, 1990). This analyzes the kinetics of the whole of oxidative phosphorylation divided into three modules connected by their common substrate or product, $\Delta\psi$. The modules are (i) the reactions that produce $\Delta\psi$, consisting of the substrate translocases, dehydrogenases and other enzymes and the components of the respiratory chain, called 'substrate oxidation'; (ii) the reactions that consume $\Delta\psi$ and synthesize, export and dephosphorylate ATP, consisting of ATP synthase, the phosphate and adenine nucleotide translocases and any ATPases that may be present, called the 'phosphorylating system'; and (iii) the reactions that consume $\Delta\psi$ without ATP synthesis, called the 'proton leak' (Brand, 1990). The analysis reports changes anywhere within oxidative phosphorylation that are functionally important but is unresponsive to changes that have no functional consequences. Comparison of the kinetic responses of each of the three modules to $\Delta\psi$ obtained using mitochondria isolated from PINK1$^{+/+}$ and PINK1$^{-/-}$ MEFs would reveal any effects of PINK1 on the kinetics of oxidative phosphorylation. Oxygen consumption and $\Delta\psi$ were measured simultaneously using mitochondria incubated with 80 ng/ml nigericin and 4 μM rotenone. Respiration was initiated by 5 mM succinate. The kinetic behavior of a '$\Delta\psi$-producer' can be established by specific modulation of a $\Delta\psi$-consumer and the kinetics of a consumer can be established by specific modulation of a $\Delta\psi$-producer (Brand, 1998). To measure the kinetic response of proton leak to $\Delta\psi$, the State 4 (non-phosphorylating) respiration of mitochondria in the presence of oligomycin (0.8 μg/ml; to prevent any residual ATP synthesis), which was used solely to drive the proton leak, was titrated with malonate (up to 8 mM). In a similar way, State 4 respiration was titrated by FCCP (up to 1 μM) for measurement of the kinetic response of substrate oxidation to $\Delta\psi$. State 3 (maximal rate of ATP synthesis) was obtained by addition of excess ADP (1 mM). Titration of State 3 respiration with malonate (up to 1.1 mM) allowed measurement of the kinetics of the $\Delta\psi$-consumers (the sum of the phosphorylating system and proton leak). The coupling efficiencies of oxidative phosphorylation were calculated from the kinetic curves as the percentage of mitochondrial respiration rate at a given $\Delta\psi$ that was used for ATP synthesis and was therefore inhibited by oligomycin. Note that any slip reactions will appear as proton leak in this analysis (Brand et al., 1994).

Mitochondrial ROS production

Mitochondrial ROS production rate was assessed by measurement of H_2O_2 generation rate, determined fluorometrically by measurement of oxidation of Amplex Red to fluorescent resorufin coupled to the enzymatic reduction of H_2O_2 by horseradish peroxidase using a spectrofluorometer RF-5300PC (Shimadzu, Kyoto, Japan). The H_2O_2 generation rate was measured in non-phosphorylating conditions (=State 4) using either pyruvate/malate or succinate as respiratory substrates. Mitochondria were incubated at 0.1 mg/ml in respiration buffer. All incubations also contained 5 μM Amplex Red, 2 U/ml horseradish peroxidase and 8 U/ml superoxide dismutase. The reaction was initiated by addition of 5 mM succinate or 4 mM pyruvate + 1 mM malonate and the increase in fluorescence was followed at excitation and emission wavelengths of 560 and 590 nm, respectively. Appropriate correction for background signals and standard curves generated using known amounts of H_2O_2 were used to calculate the rate of H_2O_2 production in nmol/min/mg mitochondrial protein. The percentage free radical leak, which is a measure of the number of electrons that produce superoxide (and subsequently H_2O_2) compared with the total number of electrons which pass thorough the respiratory chain, was calculated as the rate of H_2O_2 production divided by the rate of O_2 consumption (Barja et al., 1994).

Statistics

Values are presented as means ± SEM except Fig. 2D, in which error bars indicate SD. The significance of differences between means was assessed by the unpaired Student's *t*-test using Microsoft Excel; *P* values <0.05 were taken to be significant.

Results

Cell growth and mitochondrial morphology

In general, cultured cells gain their energy mostly from glycolysis. Therefore, cells deficient in respiratory function can grow in normal medium, although possibly at a slower rate, relying predominantly on glycolysis (Hofhaus et al., 1996). Actually, ρ^0 cells, which lack mitochondrial DNA completely, can grow producing energy exclusively through glycolysis (King and Attardi, 1989). On the other hand, galactose metabolism via glycolysis is much slower than glucose metabolism (Reitzer et al., 1979). Therefore, cells in galactose medium are forced to oxidize pyruvate through the mitochondrial respiratory chain for energy required for growth. Consequently, cells with defects in their mitochondrial respiratory chains show growth impairments in galactose medium. To evaluate this phenomenon is also observed in our cells, we examined growth retardation by addition of mitochondrial complex I inhibitor, rotenone (Fig. 1A). In glucose medium, 10 nM rotenone had only a slight effect on the growth of PINK1$^{+/+}$ MEFs and slower growth was observed even in the presence of 100 nM rotenone. However, in the galactose medium, 10 nM rotenone significantly inhibited the growth of PINK1$^{+/+}$ MEFs and 100 nM roteone completely arrested the growth. Therefore, we could confirm that the growth impairment of our cells in the galactose medium was due to mitochondrial respiratory chain defects.

PINK1 acts upstream of parkin, regulating mitochondrial integrity and function; therefore, loss of PINK1 is considered to affect mitochondrial functions. To assess the mitochondrial functions of PINK1$^{-/-}$ MEFs, growth capability in a medium in which galactose replaced glucose was examined. As shown in Fig. 1B, PINK1$^{-/-}$ MEFs appeared to show clear growth impairments in the galactose medium, whereas PINK1$^{+/+}$ MEFs grew slightly slower than in the glucose medium.

No differences of mitochondrial morphology between PINK1$^{+/+}$ and $^{-/-}$ MEFs in the glucose medium were detected (Fig. 1C), consistent with the previous report (Matsuda et al., 2010). However, in the galactose medium, mitochondria of the PINK1$^{-/-}$ MEFs were more fragmented compared to the PINK$^{+/+}$ MEFs (Fig. 1C). This is consistent with previous reports, which found mitochondrial morphological changes were more pronounced when PINK1 knock-down HeLa cells were grown in low-glucose medium (Exner et al., 2007) and human PINK1 homozygous mutant fibroblast in galactose medium (Grünewald et al., 2009). In these cells, mitochondrial morphological changes were associated with the mitochondrial functional impairment.

Assessments of mitochondrial functions at the cellular level

Because PINK1$^{-/-}$ MEFs showed severe growth impairments in the galactose medium, the mitochondrial functions of these cells were assessed at the cellular level. First, cellular respiration rates were measured (Fig. 2A). The basal respiration rate was significantly reduced in PINK1$^{-/-}$ cells compared with that in PINK1$^{+/+}$ cells (11.13 ± 0.71 versus 14.36 ± 1.01 nmol O/min/10^6 cells; $p<0.05$; $n=5$ independent experiments), consistent with previous reports using partial knock-down of PINK1 expression (Gandhi et al., 2009; Liu et al., 2009). Oligomycin inhibits ATP synthase, resulting in non-phosphorylating respiration. FCCP uncouples oxidative phosphorylation, leading to maximum respiration rates. In both conditions, the

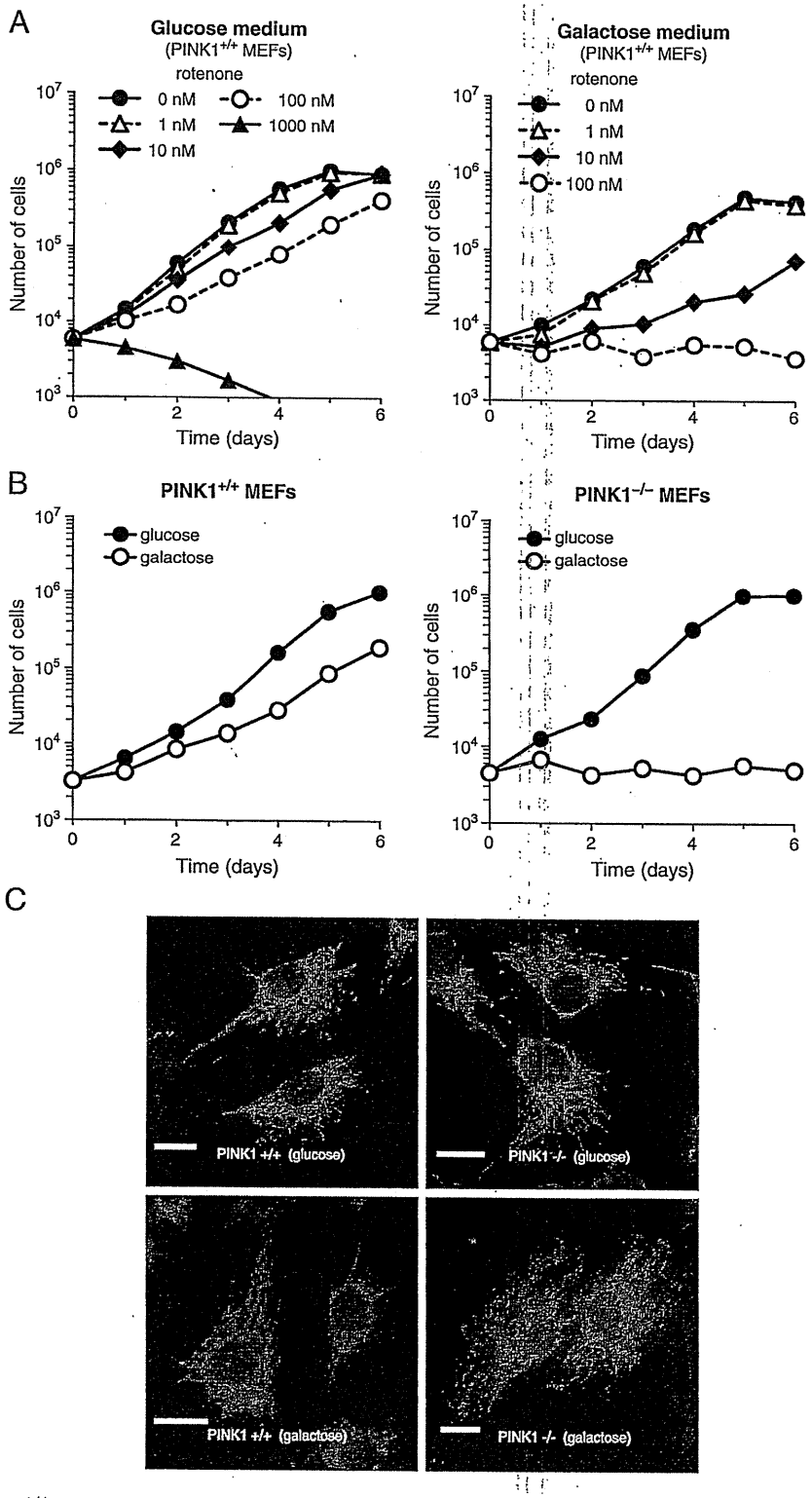

Fig. 1. (A) Growth retardation of PINK1$^{+/+}$ MEFs by mitochondrial complex I inhibitor, rotenone in glucose or galactose medium. Closed circles with solid line, 0 nM rotenone; open triangles with dashed line, 1 nM rotenone; closed diamonds with solid line, 10 nM rotenone; open circles with dashed line, 100 nM rotenone; closed triangles with solid line, 1000 nM rotenone. Cells grown in 12-well plates were trypsinized and live cells were assessed by trypan blue dye exclusion. (B) Growth curves of PINK1$^{+/+}$ and $^{-/-}$ MEFs. Closed symbols (*glucose*), growth curve for cells grown in DMEM containing 4.5 g/l glucose and 1 mM sodium pyruvate; open symbols (*galactose*), growth curve for cells grown in DMEM lacking glucose and containing instead 1.0 g/l galactose and 1 mM sodium pyruvate. Cells grown in 12-well plates were trypsinized and live cells were assessed by trypan blue dye exclusion. (C) Mitochondrial morphology of PINK1$^{+/+}$ and $^{-/-}$ MEFs. After incubating cells with the glucose or galactose medium for 24 hours, cells were fixed and immunostained with anti-Tom20 antibody to visualize mitochondria. Scale bar, 20 μm.

PINK1$^{-/-}$ cells respired significantly slower than the PINK1$^{+/+}$ cells (1.76 ± 0.13 versus 2.95 ± 0.27 ($p<0.01$; $n=5$ independent experiments) and 16.44 ± 1.80 versus 23.50 ± 1.18 nmol O/min/10^6 cells ($p<0.05$; $n=5$ independent experiments), respectively).

The main function of mitochondria is ATP synthesis via oxidative phosphorylation. ATP levels under basal conditions were significantly reduced in PINK1$^{-/-}$ MEFs (Fig. 2B), as reported previously for dissociated PINK1$^{-/-}$ mouse neurons (Gispert et al., 2009) and PINK1

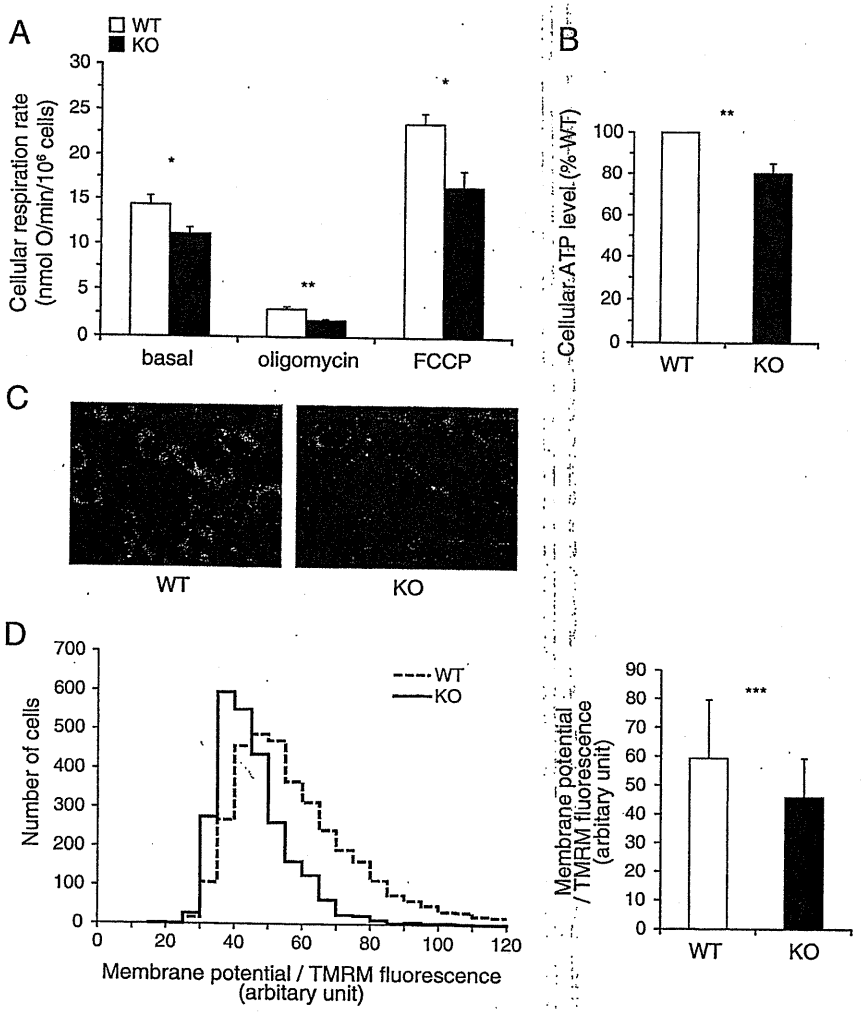

Fig. 2. Mitochondrial functions assessed at the cellular level. Open bars, PINK1$^{+/+}$ MEFs; closed bars, PINK1$^{-/-}$ MEFs. (A) Cell respiration rate of PINK1$^{+/+}$ and $^{-/-}$ MEFs. The oxygen respiration rate was measured at density of 8.0×10^6 cells/ml under each of the following three conditions: basal rate (no additions); State 4 (no ATP synthesis) [after addition of 1 μg/ml oligomycin], uncoupled [after addition of 3 μM FCCP]. After sequential measurements, the endogenous respiration rate was determined by adding 1 μM rotenone + 2 μM myxothiazol. Error bars indicate SEM ($n=5$ independent experiments). (B) Cellular ATP levels. Data were normalized based on cell numbers and expressed as the percentage of the level in PINK1$^{+/+}$ cells. Error bars indicate SEM ($n=4$ independent experiments). (C) Live cell images of PINK1$^{+/+}$ and $^{-/-}$ MEFs with TMRM fluorescence. (D) Mitochondrial membrane potential evaluated by live cell imaging of TMRM fluorescence. *Left panel*, the distribution of TMRM fluorescence from 3537 PIINK1$^{+/+}$ and 2566 PINK1$^{-/-}$ cells from 12 wells per cell type; *right panel*, the average value of TMRM fluorescence per cell. Error bars indicate SD. *$P<0.05$; **$P<0.01$; ***$P<0.001$.

siRNA knock-down PC12 cells (Liu et al., 2009). Mitochondrial membrane potential was also measured by live cell imaging of TMRM fluorescence. Typical images were shown in Fig. 2C. The histogram shows the distribution of TMRM fluorescence from 3537 PINK1$^{+/+}$ cells and 2566 PINK1$^{-/-}$ cells from 12 wells per cell type and the bar graph indicates the mean ± SD of TMRM fluorescence per cell (Fig. 2D). According to the Nernst equation, the ratio of TMRM fluorescence would translate into, on average, 6.88 mV lower mitochondrial membrane potential in the PINK1$^{-/-}$ cells if the plasma membrane potentials were not different between PINK1$^{+/+}$ and $^{-/-}$ cells. Mitochondrial membrane potential decrease was also showed previously in PINK1 knock-down HeLa cells (Exner et al., 2007) and in stable PINK1 knock-down neuroblastoma cell lines (Sandebring et al., 2009).

Assessments of mitochondrial functions using isolated mitochondria

To further analyze mitochondrial functions, we measured the kinetics of oxidative phosphorylation using isolated mitochondria from PINK1$^{+/+}$ and $^{-/-}$ MEFs. Fig. 3 shows the kinetics of the three modules of oxidative phosphorylation using succinate as a respiratory substrate (complex II-linked respiration). Fig. 3A shows the kinetic response of substrate oxidation to its product, $\Delta\psi$. The substrate oxidation kinetic curve for PINK1$^{-/-}$ cells was clearly shifted lower compared with that for PINK1$^{+/+}$ cells, indicating that the loss of PINK1 caused mitochondrial respiratory chain defects. Fig. 3B shows the kinetic response of proton leak to its driving force, $\Delta\psi$, and Fig. 3C shows the kinetic response of the ATP phosphorylating pathway to its driving force, $\Delta\psi$. Both kinetic curves for PINK1$^{+/+}$ and $^{-/-}$ MEFs (open and closed symbols, respectively) were overlapping, implying that there were no significant differences in those modules.

We also independently measured the mitochondrial oxygen consumption rate using pyruvate/malate as a respiratory substrate instead of succinate to check complex I. Modular kinetic analysis using pyruvate/malate is technically difficult for the following reasons: (1) the oxygen consumption rate with pyruvate/malate is much slower than succinate respiration; and (2) there are no competitive inhibitors of complex I-linked respiration, such as malonate for succinate respiration. As shown in Fig. 4A, the respiration rates in State 3 and 4 with pyruvate/malate of isolated mitochondria from PINK1$^{-/-}$ cells (closed symbols) were significantly slower than those of PINK1$^{+/+}$ cells (open symbols), as in the case of succinate respiration (Fig. 4B; data derived from the kinetic curves in Fig. 3).

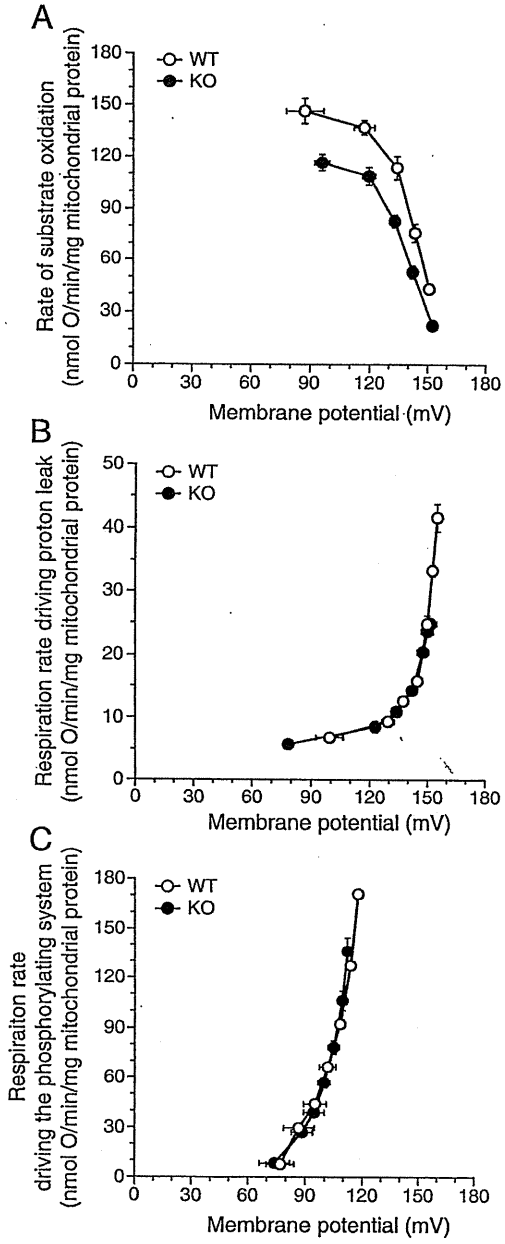

Fig. 3. Modular kinetic analysis of oxidative phosphorylation in mitochondria isolated from PINK1$^{+/+}$ and $^{-/-}$ MEFs. Modular kinetic analysis of the kinetic responses to membrane potential, $\Delta\psi$, of respiration driving (A) substrate oxidation ($\Delta\psi$ titrated with uncoupler, FCCP, starting in State 4), (B) proton leak ($\Delta\psi$ titrated with malonate, starting in State 4) and (C) the phosphorylating system, calculated by subtracting respiration driving proton leak from respiration driving the $\Delta\psi$-consumers ($\Delta\psi$ titrated with malonate starting in State 3; not shown) at each $\Delta\psi$. Open symbols, PINK1$^{+/+}$ MEFs; closed symbols, PINK1$^{-/-}$ MEFs. Error bars indicate SEM ($n=4$ independent mitochondrial preparations).

Mitochondrial ROS production

Mitochondrial ROS production rate was assessed by measurement of the H_2O_2 generation rate. Mechanisms of mitochondrial ROS production were well described elsewhere (Fig. 1 of Lambert et al., 2010). Pyruvate and malate generate NADH, which induced forward electron transport and generate ROS mainly from complex I and III. For pyruvate/malate respiration, the basal H_2O_2 generation rate (measured in the absence of respiratory chain inhibitors) was not different between PINK1$^{+/+}$ and $^{-/-}$ mitochondria (Fig. 4C). The addition of antimycin A and further addition of rotenone, which inhibited forward electron transport at complex III and I, respectively, enhanced H_2O_2 generation. During succinate respiration in the absence of respiratory chain inhibitors, ROS are generated mainly from the quinine binding site of complex I due to reverse electron flow from coenzyme Q to complex I. For succinate respiration, H_2O_2 generation rate in the absence of reparatory chain inhibitors was higher in PINK1$^{+/+}$ mitochondria than in PINK1$^{-/-}$ mitochondria, but the difference was not significant (Fig. 4D). The addition of rotenone, which blocks reverse electron flow from coenzyme Q to complex I, attenuated H_2O_2 generation.

Figs. 4 C and D show a tendency for PINK1$^{+/+}$ mitochondria to generate more ROS than PINK1$^{-/-}$ mitochondria. However, their respiration rates were remarkably different (Figs. 4A and B). Therefore, we calculated the percentage free radical leak, which is the fraction of molecules of O_2 consumed that give rise to H_2O_2 release by mitochondria (free radical leak) during either pyruvate/malate or succinate State 4 respiration (Figs. 4E and F). For pyruvate/malate respiration, mitochondria isolated from PINK1$^{-/-}$ cells had higher proportion of H_2O_2 generation than PINK1$^{+/+}$ mitochondria. During succinate respiration without respiratory inhibitors, PINK1$^{-/-}$ mitochondria had also higher proportion of free radical leak mainly from complex I due to reverse electron flow from coenzyme Q to complex I. Because the differences disappeared with addition of rotenone, which inhibit reverse electron flow, ROS generation enhanced by loss of PINK1 was mostly from complex I.

Discussion

We produced an *in vitro* model of Parkinson's disease, immortalized PINK1$^{-/-}$ MEFs. Previously, impairment of mitochondrial respiration was observed in the brains of PINK1$^{-/-}$ mice (Gautier et al., 2008). PINK1$^{-/-}$ MEFs clearly showed a phenotype of mitochondrial dysfunctions, which is consistent with PD pathogenesis. This phenotype was apparent in a cell growth experiment using medium containing galactose instead of glucose (Fig. 1B). Mitochondrial fragmentation was observed when PINK1$^{-/-}$ MEFs grew in the galactose medium (Fig. 1C), which was consistent with previous reports (Exner et al., 2007; Grünewald et al., 2009). Our results have unveiled that the PINK1$^{-/-}$ MEF line could be a potential PD model, presenting growth retardation due to decreased mitochondrial respiration activity. Thus, the PINK1$^{-/-}$ MEFs are a useful tool for evaluating the role of PINK1 in mitochondrial dysfunction and relevant to PD.

In PINK1$^{-/-}$ MEFs, mitochondrial membrane potential was decreased compared with that in littermate wild-type MEFs (Figs. 2C and D), as reported previously for PINK1 knock-down HeLa cells (Exner et al., 2007) and stable PINK1 knock-down neuroblastoma cell lines (Sandebring et al., 2009). This is a key event during elimination of mitochondria. Mitochondrial fission followed by selective fusion segregates damaged mitochondria, which decreases their membrane potential, and permits their removal by autophagy (Twig et al., 2008). The PINK1–parkin pathway is thought to have a crucial role in this mitochondrial elimination mechanism (Geisler et al., 2010; Kawajiri et al., 2010; Matsuda et al., 2010; Narendra et al., 2008, 2010; Vives-Bauza et al., 2010). To clarify what caused the decrease in mitochondrial membrane potential, we performed a modular kinetic analysis using isolated mitochondria (Fig. 3). This analyzes the kinetics of the whole of oxidative phosphorylation divided into three modules connected by their common substrate or product, mitochondrial membrane potential ($\Delta\psi$). The modules are include one $\Delta\psi$-producer (substrate oxidation) and two $\Delta\psi$-consumers (phosphorylating system and proton leak) (Brand, 1990). To decrease $\Delta\psi$, the $\Delta\psi$-producer should be down-regulated and/or $\Delta\psi$-consumers should be up-regulated. As cellular ATP levels were decreased compared with those in littermate wild-type MEFs (Fig. 2B), it is unlikely that the phosphorylating system is up-regulated. Indeed, the kinetics of the phosphorylation module were not altered (Fig. 3C). The other $\Delta\psi$-consumer, proton leak,

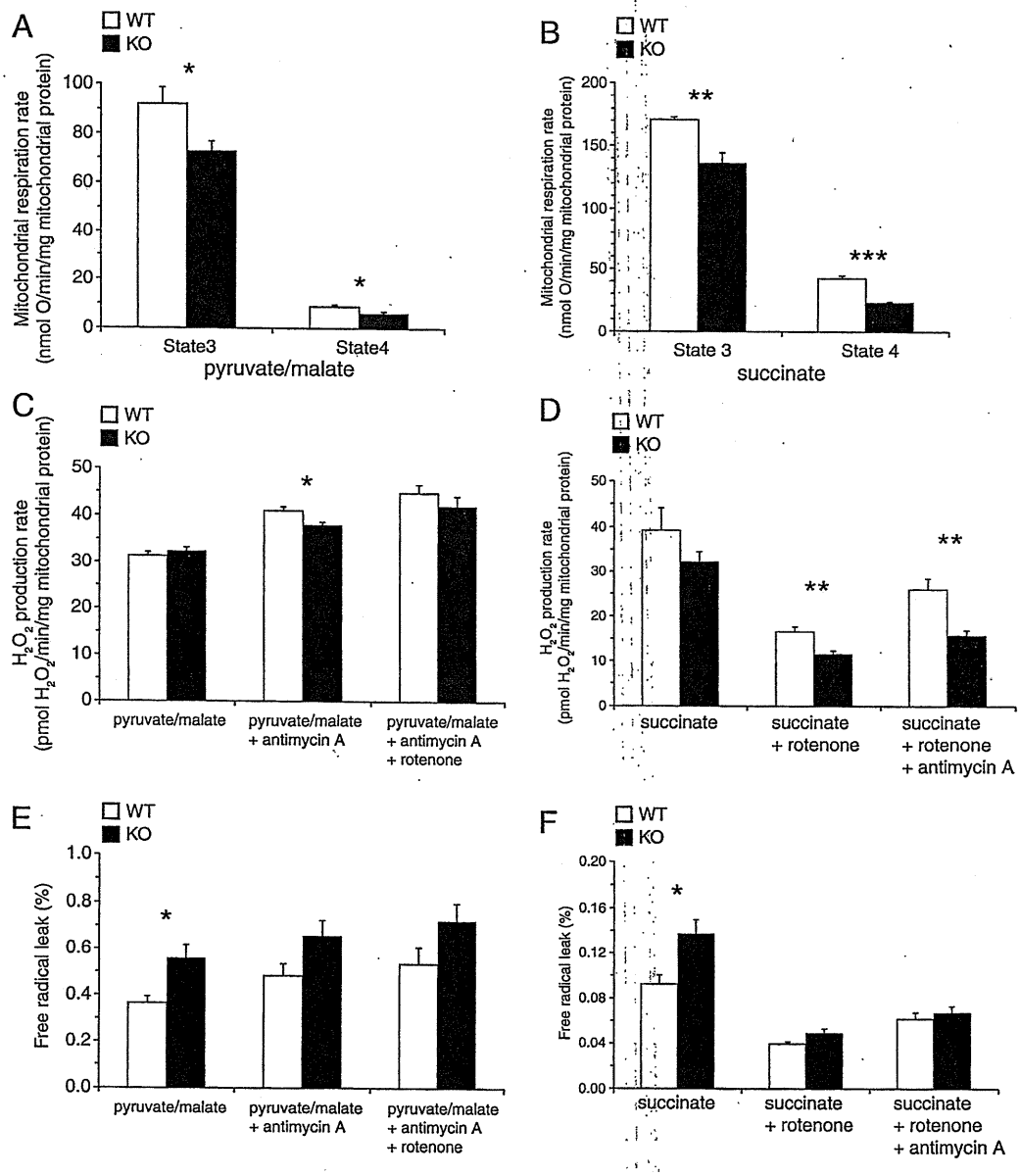

Fig. 4. Oxygen consumption rate and H_2O_2 production rate of mitochondria isolated from PINK1$^{+/+}$ and $^{-/-}$ MEFs. Open bars, PINK1$^{+/+}$ MEFs; closed bars, PINK1$^{-/-}$ MEFs. (A) State 3 and State 4 respiration rate of mitochondria with pyruvate/malate as a respiratory substrate. (B) State 3 and State 4 respiration rate of mitochondria with succinate as a respiratory substrate. Data were derived from the results of modular kinetic analysis (Fig. 3). State 3 respiration rates were the kinetic start points of the $\Delta\psi$-consumers (the sum of the phosphorylating system and proton leak). State 4 respiration rates were average values of the respiration rates at the kinetic start points of substrate oxidation and proton leak. (C, D) Mitochondrial H_2O_2 production rate with pyruvate/malate (C) or succinate (D) as a respiratory substrate. (E, F) Percentage free radical leak (FRL) for State 4 respiration with pyruvate/malate (E) or succinate (F) as a respiratory substrate. Error bars indicate SEM ($n=5$ and 4 independent mitochondrial preparations for pyruvate/malate and succinate respiration, respectively). *$P<0.05$; **$P<0.01$; ***$P<0.001$.

which partially dissipates the membrane potential without ATP synthesis, was also not changed (Fig. 3B). Therefore, the decrease in membrane potential caused by loss of PINK1 is likely to have been caused only by lower activity of the $\Delta\psi$-producer, substrate oxidation (Fig. 3A). This is the first report showing that mitochondrial membrane potential decrease caused by loss of PINK1, which is the key event for the following mitochondrial elimination, was not due to proton leak, but to respiratory chain defects. We used only succinate (a complex II-linked substrate) as a respiratory substrate in the modular kinetic analysis for technical reasons. However, complex I-linked respiration (pyruvate/malate) was also decreased in PINK1$^{-/-}$ MEFs like succinate respiration (Fig. 4A).

The mitochondrial respiration rates in State 4 were decreased in PINK1$^{-/-}$ MEFs, and consequently, the proportions of free radical leak were significantly higher in PINK1$^{-/-}$ MEFs than in PINK1$^{+/+}$ MEFs (Figs. 4E and F). Because the differences disappeared with addition of rotenone (complex I inhibitor, which inhibits reverse electron flow from coenzyme Q to complex I), ROS generation enhanced by loss of PINK1 was mostly from complex I. These results are partially consistent with those in previous reports, suggesting that MPTP and rotenone induce neuronal cell death by inhibiting complex I activity, leading to a PD-like phenotype (Dauer and Przedborski, 2003; Jackson-Lewis and Przedborski, 2007; Trojanowski, 2003).

In this study, we developed an *in vitro* PD model, the PINK1$^{-/-}$ MEF line, and established the experimental conditions for cell growth to detect mitochondrial dysfunction. This is the first report showing that complete ablation of PINK1 causes a decrease in mitochondrial membrane potential, which is not due to proton leak, but to respiratory chain defects.

Supplementary materials related to this article can be found online at doi:10.1016/j.nbd.2010.08.027.

Acknowledgments

This work was supported by a Grant-in-Aid for Scientific Research for Young Scientists (B) from JSPS (T.A. and S.Saiki), a JSPS fellowship (T.A.), Nagao Memorial Fund (S. Saiki) and a Grant from Takeda Scientific Foundation (S. Saiki and T.A.). We thank Dr. Noriyuki Matsuda for assistance to obtain immortalized cells.

References

Abou-Sleiman, P.M., Muqit, M.M., Wood, N.W., 2006. Expanding insights of mitochondrial dysfunction in Parkinson's disease. Nat. Rev. Neurosci. 7, 207–219.
Amo, T., Brand, M.D., 2007. Were inefficient mitochondrial haplogroups selected during migrations of modern humans? A test using modular kinetic analysis of coupling in mitochondria from cybrid cell lines. Biochem. J. 404, 345–351.
Barja, G., Cadenas, S., Rojas, C., Pérez-Campo, R., López-Torres, M., 1994. Low mitochondrial free radical production per unit O_2 consumption can explain the simultaneous presence of high longevity and high aerobic metabolic rate in birds. Free Radic. Res. 21, 317–327.
Brand, M.D., 1990. The proton leak across the mitochondrial inner membrane. Biochim. Biophys. Acta 1018, 128–133.
Brand, M.D., 1995. Measurement of mitochondrial protonmotive force. In: Brown, G.C., Cooper, C.E. (Eds.), Bioenergetics, a practical approach. IRL Press, Oxford, pp. 39–62.
Brand, M.D., 1998. Top-down elasticity analysis and its application to energy metabolism in isolated mitochondria and intact cells. Mol. Cell. Biochem. 184, 13–20.
Brand, M.D., Chien, L.F., Diolez, P., 1994. Experimental discrimination between proton leak and redox slip during mitochondrial electron transport. Biochem. J. 297, 27–29.
Chu, C.T., 2010. Tickled PINK1: mitochondrial homeostasis and autophagy in recessive Parkinsonism. Biochim. Biophys. Acta 1802, 20–28.
Clark, I.E., Dodson, M.W., Jiang, C., Cao, J.H., Huh, J.R., Seol, J.H., Yoo, S.J., Hay, B.A., Guo, M., 2006. *Drosophila pink1* is required for mitochondrial function and interacts genetically with *parkin*. Nature 441, 1162–1166.
Dauer, W., Przedborski, S., 2003. Parkinson's disease: mechanisms and models. Neuron 39, 889–909.
Exner, N., Treske, B., Paquet, D., Holmstrom, K., Schiesling, C., Gispert, S., Carballo-Carbajal, I., Berg, D., Hoepken, H.H., Gasser, T., Krüger, R., Winklhofer, K.F., Vogel, F., Reichert, A.S., Auburger, G., Kahle, P.J., Schmid, B., Haass, C., 2007. Loss-of-function of human PINK1 results in mitochondrial pathology and can be rescued by parkin. J. Neurosci. 27, 12413–12418.
Gandhi, S., Wood-Kaczmar, A., Yao, Z., Plun-Favreau, H., Deas, E., Klupsch, K., Downward, J., Latchman, D.S., Tabrizi, S.J., Wood, N.W., Duchen, M.R., Abramov, A.Y., 2009. PINK1-associated Parkinson's disease is caused by neuronal vulnerability to calcium-induced cell death. Mol. Cell 33, 627–638.
Gautier, C.A., Kitada, T., Shen, J., 2008. Loss of PINK1 causes mitochondrial functional defects and increased sensitivity to oxidative stress. Proc. Natl. Acad. Sci. U. S. A. 105, 11364–11369.
Geisler, S., Holmström, K.M., Skujat, D., Fiesel, F.C., Rothfuss, O.C., Kahle, P.J., Springer, W., 2010. PINK1/Parkin-mediated mitophagy is dependent on VDAC1 and p62/SQSTM1. Nat. Cell Biol. 12, 119–131.
Gispert, S., Ricciardi, F., Kurz, A., Azizov, M., Hoepken, H.H., Becker, D., Voos, W., Leuner, K., Müller, W.E., Kudin, A.P., Kunz, W.S., Zimmermann, A., Roeper, J., Wenzel, D., Jendrach, M., García-Arencíbia, M., Fernández-Ruiz, J., Huber, L., Rohrer, H., Barrera, M., Reichert, A.S., Rüb, U., Chen, A., Nussbaum, R.L., Auburger, G., 2009. Parkinson phenotype in aged PINK1-deficient mice is accompanied by progressive mitochondrial dysfunction in absence of neurodegeneration. PLoS One 4, e5777.
Grünewald, A., Gegg, M.E., Taanman, J.W., King, R.H., Kock, N., Klein, C., Schapira, A.H., 2009. Differential effects of PINK1 nonsense and missense mutations on mitochondrial function and morphology. Exp. Neurol. 219, 266–273.
Haque, M.E., Thomas, K.J., D'Souza, C., Callaghan, S., Kitada, T., Slack, R.S., Fraser, P., Cookson, M.R., Tandon, A., Park, D.S., 2008. Cytoplasmic Pink1 activity protects neurons from dopaminergic neurotoxin MPTP. Proc. Natl. Acad. Sci. U. S. A. 105, 1716–1721.
Hofhaus, G., Johns, D.R., Hurko, O., Attardi, G., Chomyn, A., 1996. Respiration and growth defects in transmitochondrial cell lines carrying the 11778 mutation associated with Leber's hereditary optic neuropathy. J. Biol. Chem. 271, 13155–13161.
Jackson-Lewis, V., Przedborski, S., 2007. Protocol for the MPTP mouse model of Parkinson's disease. Nat. Protoc. 2, 141–151.
Kawajiri, S., Saiki, S., Sato, S., Sato, F., Hatano, T., Eguchi, H., Hattori, N., 2010. PINK1 is recruited to mitochondria with parkin and associates with LC3 in mitophagy. FEBS Lett. 584, 1073–1079.
Kim, Y., Park, J., Kim, S., Song, S., Kwon, S.K., Lee, S.H., Kitada, T., Kim, J.M., Chung, J., 2008. PINK1 controls mitochondrial localization of Parkin through direct phosphorylation. Biochem. Biophys. Res. Commun. 377, 975–980.
King, M.P., Attardi, G., 1989. Human cells lacking mtDNA: repopulation with exogenous mitochondria by complementation. Science 246, 500–503.
Lambert, A.J., Buckingham, J.A., Boysen, H.M., Brand, M.D., 2010. Low complex I content explains the low hydrogen peroxide production rate of heart mitochondria from the long-lived pigeon, Columba livia. Aging Cell 9, 78–91.
Liu, W., Vives-Bauza, C., Acin-Perez, R., Yamamoto, A., Tan, Y., Li, Y., Magrane, J., Stavarache, M.A., Shaffer, S., Chang, S., Kaplitt, M.G., Huang, X.Y., Beal, M.F., Manfredi, G., Li, C., 2009. PINK1 defect causes mitochondrial dysfunction, proteasomal deficit and alpha-synuclein aggregation in cell culture models of Parkinson's disease. PLoS One 4, e4597.
Matsuda, N., Sato, S., Shiba, K., Okatsu, K., Saisho, K., Gautier, C.A., Sou, Y.S., Saiki, S., Kawajiri, S., Sato, F., Kimura, M., Komatsu, M., Hattori, N., Tanaka, K., 2010. PINK1 stabilized by mitochondrial depolarization recruits Parkin to damaged mitochondria and activates latent Parkin for mitophagy. J. Cell Biol. 189, 211–221.
Narendra, D., Tanaka, A., Suen, D.F., Youle, R.J., 2008. Parkin is recruited selectively to impaired mitochondria and promotes their autophagy. J. Cell Biol. 183, 795–803.
Narendra, D.P., Jin, S.M., Tanaka, A., Suen, D.F., Gautier, C.A., Shen, J., Cookson, M.R., Youle, R.J., 2010. PINK1 is selectively stabilized on impaired mitochondria to activate Parkin. PLoS Biol. 8, e1000298.
Park, J., Lee, S.B., Lee, S., Kim, Y., Song, S., Kim, S., Bae, E., Kim, J., Shong, M., Kim, J.M., Chung, J., 2006. Mitochondrial dysfunction in *Drosophila PINK1* mutants is complemented by *parkin*. Nature 441, 1157–1161.
Pridgeon, J.W., Olzmann, J.A., Chin, L.S., Li, L., 2007. PINK1 protects against oxidative stress by phosphorylating mitochondrial chaperone TRAP1. PLoS Biol. 5, e172.
Reitzer, L.J., Wice, B.M., Kennell, D., 1979. Evidence that glutamine, not sugar, is the major energy source for cultured HeLa cells. J. Biol. Chem. 254, 2669–2676.
Reynafarje, B., Costa, L.E., Lehninger, A.L., 1985. O_2 solubility in aqueous media determined by a kinetic method. Anal. Biochem. 145, 406–418.
Sandebring, A., Thomas, K.J., Beilina, A., van der Brug, M., Cleland, M.M., Ahmad, R., Miller, D.W., Zambrano, I., Cowburn, R.F., Behbahani, H., Cedazo-Mínguez, A., Cookson, M.R., 2009. Mitochondrial alterations in PINK1 deficient cells are influenced by calcineurin-dependent dephosphorylation of dynamin-related protein 1. PLoS One 4, e5701.
Trojanowski, J.Q., 2003. Rotenone neurotoxicity: a new window on environmental causes of Parkinson's disease and related brain amyloidoses. Exp. Neurol. 179, 6–8.
Twig, G., Elorza, A., Molina, A.J., Mohamed, H., Wikstrom, J.D., Walzer, G., Stiles, L., Haigh, S.E., Katz, S., Las, G., Alroy, J., Wu, M., Py, B.F., Yuan, J., Deeney, J.T., Corkey, B. E., Shirihai, O.S., 2008. Fission and selective fusion govern mitochondrial segregation and elimination by autophagy. EMBO J. 27, 433–446.
Valente, E.M., Abou-Sleiman, P.M., Caputo, V., Muqit, M.M., Harvey, K., Gispert, S., Ali, Z., Del Turco, D., Bentivoglio, A.R., Healy, D.G., Albanese, A., Nussbaum, R., González-Maldonado, R., Deller, T., Salvi, S., Cortelli, P., Gilks, W.P., Latchman, D.S., Harvey, R.J., Dallapiccola, B., Auburger, G., Wood, N.W., 2004. Hereditary early-onset Parkinson's disease caused by mutations in *PINK1*. Science 304, 1158–1160.
Vives-Bauza, C., Zhou, C., Huang, Y., Cui, M., de Vries, R.L., Kim, J., May, J., Tocilescu, M.A., Liu, W., Ko, H.S., Magrane, J., Moore, D.J., Dawson, V.L., Grailhe, R., Dawson, T.M., Li, C., Tieu, K., Przedborski, S., 2010. PINK1-dependent recruitment of Parkin to mitochondria in mitophagy. Proc. Natl. Acad. Sci. U. S. A. 107, 378–383.
Wood-Kaczmar, A., Gandhi, S., Yao, Z., Abramov, A.Y., Miljan, E.A., Keen, G., Stanyer, L., Hargreaves, I., Klupsch, K., Deas, E., Downward, J., Mansfield, L., Jat, P., Taylor, J., Heales, S., Duchen, M.R., Latchman, D., Tabrizi, S.J., Wood, N.W., 2008. PINK1 is necessary for long term survival and mitochondrial function in human dopaminergic neurons. PLoS One 3, e2455.
Yang, Y., Ouyang, Y., Yang, L., Beal, M.F., McQuibban, A., Vogel, H., Lu, B., 2008. Pink1 regulates mitochondrial dynamics through interaction with the fission/fusion machinery. Proc. Natl. Acad. Sci. U. S. A. 105, 7070–7075.